Received: 27 March 2024 | Accepted: 27 March 2024

DOI: 10.1111/gcb.17270

Global Change Biology WILEY

CORRIGENDUM

Correction to "Genomic architecture controls multivariate adaptation to climate change"

Terasaki Hart, D., E., & Wang, I., J. (2024). Genomic architecture controls multivariate adaptation to climate change. *Global Change Biology*, 30(2), e17179. doi: 10.1111/gcb.17179.

Figures 4, S3, and S4 show rows of data ordered identically to other paneled figures: top-to-bottom, the rows show the results for scenarios with independent, weak, and strong linkage. However, the original row labels in Figures 4, S3, and S4 were out of order, reading, top-to-bottom, "weak," "strong," and "independent." The order of these labels has now been corrected to "Independent," "Weak," "Strong," top-to-bottom. The corrected Figure 4 is below.

Also, the end of the last sentence in the section Results: Gene flow stated "differences between moderate- and high-redundancy scenarios were minor." That was a typo. It should have read "differences between moderate- and high-polygenicity scenarios were minor."

We apologize for any confusion this caused.

FIGURE 4 Scatterplots of the observed versus expected phenotypic shift during the climate change period for all 18 of our simulated scenarios. For each scenario, the left ("before") scatterplot shows the distribution of phenotypes before climate change begins, and the right ("after") scatterplot shows how the distribution has shifted by the end of the climate change period. The trait adapted to the shifting environmental gradient is distributed along the *x*-axis, with the trait adapted to the stable gradient on the *y*-axis. Each plot is an ensemble of the results for all 100 replicates of each scenario. The size and opacity of each point represent the number of individuals exhibiting that two-dimensional phenotype. The gridded arrangement of the points in each scatterplot is a function of the number of loci per trait, which determines the set of possible phenotypes. Solid black lines delineate the shifts in the phenotypic distributions' central tendencies that are expected to take place during the climate change period; dotted black lines depict the observed distributions' central tendencies; and red wedges depict the differences between the expected and observed distributions ("phenotypic shortfall").

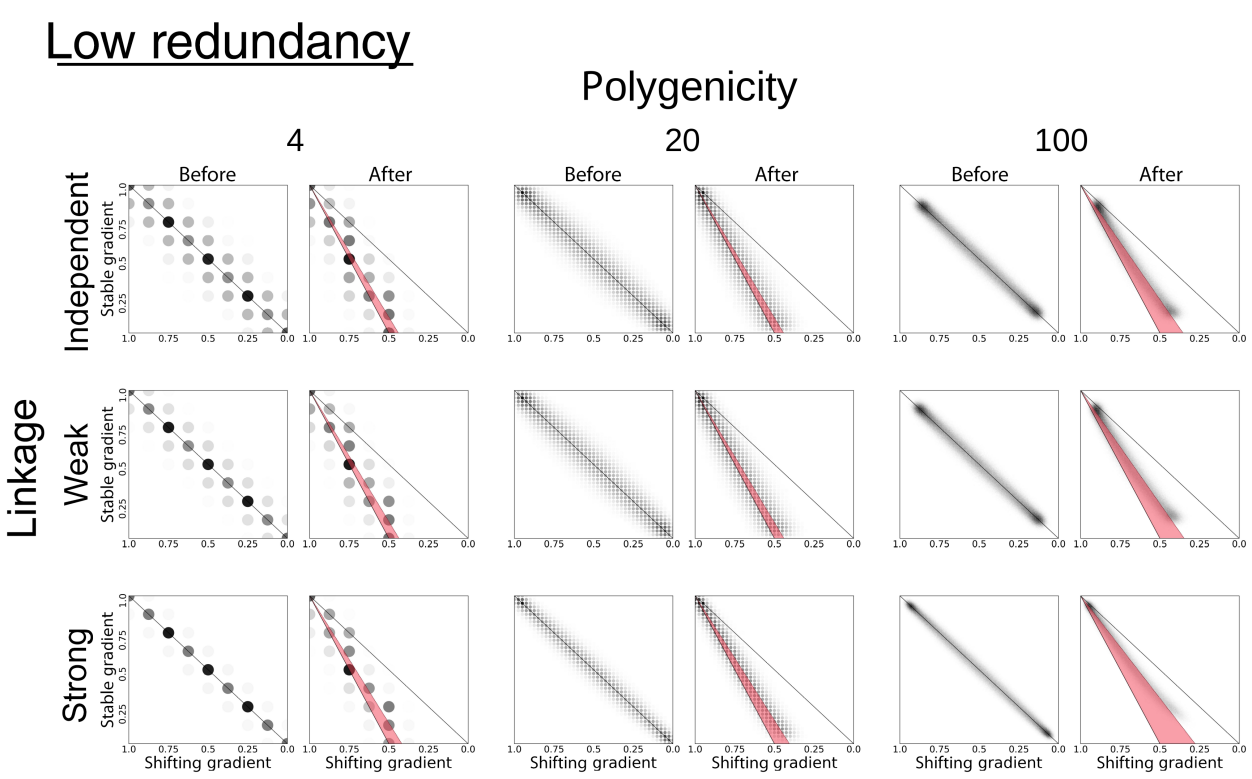

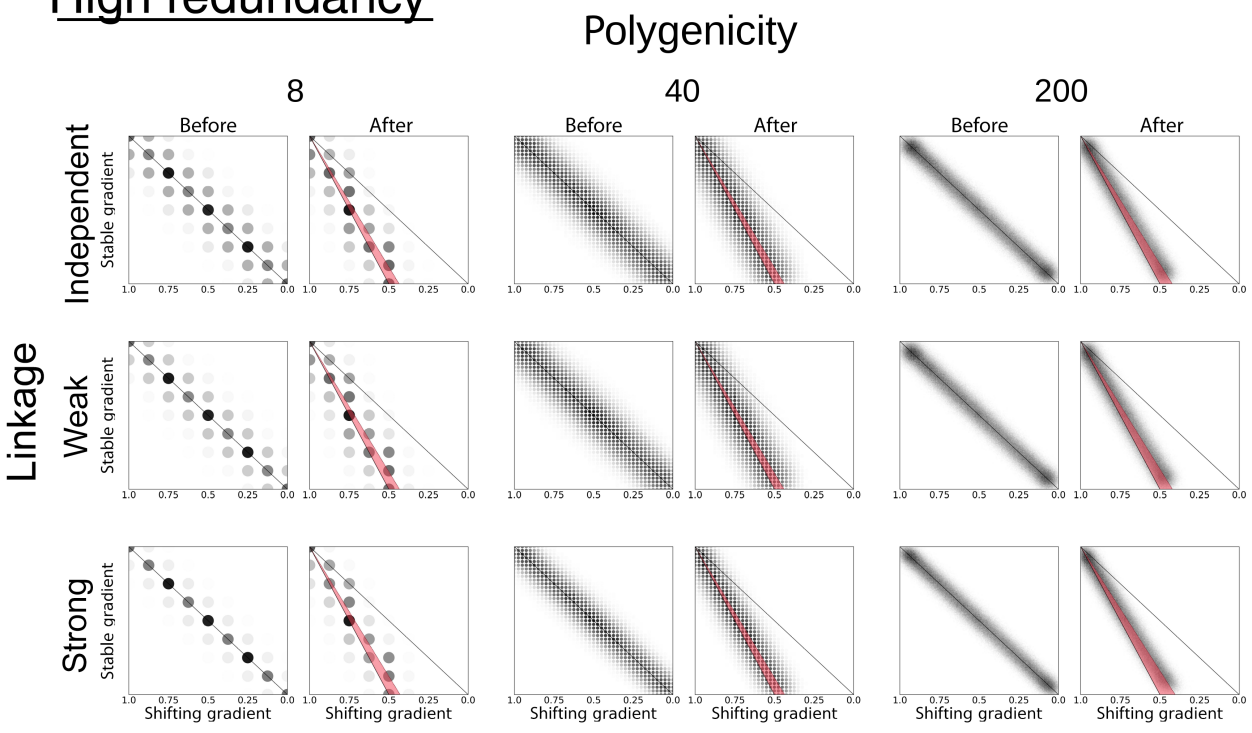

Received: 8 June 2023 | Revised: 11 December 2023 | Accepted: 12 January 2024

DOI: 10.1111/gcb.17179

Global Change Biology WILEY

RESEARCH ARTICLE

Genomic architecture controls multivariate adaptation to climate change

Drew E. Terasaki Hart[1,2,3] | Ian J. Wang[1]

[1]Department of Environmental Science, Policy, and Management, University of California, Berkeley, Berkeley, California, USA

[2]The Nature Conservancy, Arlington, Virginia, USA

[3]CSIRO Environment, Brisbane, Queensland, Australia

Correspondence
Drew E. Terasaki Hart, CSIRO Environment, Brisbane, QLD 4102, Australia.
Email: drew.terasakihart@csiro.au

Funding information
Bezos Earth Fund; Division of Environmental Biology, Grant/Award Number: DEB1845682; University of California, Berkeley

Abstract

As climate change advances, environmental gradients may decouple, generating novel multivariate environments that stress wild populations. A commonly invoked mechanism of evolutionary rescue is adaptive gene flow tracking climate shifts, but gene flow from populations inhabiting similar conditions on one environmental axis could cause maladaptive introgression when populations are adapted to different environmental variables that do not shift together. Genomic architecture can play an important role in determining the effectiveness and relative magnitudes of adaptive gene flow and in situ adaptation. This may have direct consequences for how species respond to climate change but is often overlooked. Here, we simulated microevolutionary responses to environmental change under scenarios defined by variation in the polygenicity, linkage, and genetic redundancy of two independent traits, one of which is adapted to a gradient that shifts under climate change. We used these simulations to examine how genomic architecture influences evolutionary outcomes under climate change. We found that climate-tracking (up-gradient) gene flow, though present in all scenarios, was strongly constrained under scenarios of lower linkage and higher polygenicity and redundancy, suggesting in situ adaptation as the predominant mechanism of evolutionary rescue under these conditions. We also found that high polygenicity caused increased maladaptation and demographic decline, a concerning result given that many climate-adapted traits may be polygenic. Finally, in scenarios with high redundancy, we observed increased adaptive capacity. This finding adds to the growing recognition of the importance of redundancy in mediating in situ adaptive capacity and suggests opportunities for better understanding the climatic vulnerability of real populations.

KEYWORDS
adaptation, climate change, gene flow, genetic redundancy, genomic architecture, landscape genomics, spatial simulation

1 | INTRODUCTION

Climate change is one of the foremost threats to biodiversity in the Anthropocene. The ability of species to persist within their current ranges will likely depend largely upon their abilities to locally adapt to new climate conditions—a concept frequently referred to as "adaptive capacity" or "evolutionary potential" (Chevin et al., 2010; Harrisson et al., 2014; Nicotra et al., 2015;

Vilas et al., 2015; Wade et al., 2017). Because beneficial de novo mutations take a long time to arise, this adaptation will likely be facilitated by the reconfiguration of existing adaptive genetic diversity (Bomblies & Peichel, 2022). A common conceptual model underlying this scenario is that of adaptive gene flow tracking a shifting climatic gradient (Ackerly et al., 2010; Loarie et al., 2009), which would bring beneficial genes into recipient populations from "climate-suitable" populations whose current climates approximate future local conditions (Bellis et al., 2020). This model of adaptive gene flow has both theoretical (Aitken & Whitlock, 2013; Slatkin, 1987; Tigano & Friesen, 2016) and empirical (Bell & Gonzalez, 2011; Feder et al., 2012) support but meets resistance under conditions in which gene flow can be maladaptive (Felsenstein, 1976; Haldane, 1930; Wang & Bradburd, 2014; Lenormand, 2002; Slatkin, 1987; Wright, 1931). In these circumstances, shifting allelic covariance—the in situ recombination of standing genetic variation into new, adaptive genotypes—could be a more efficient mechanism underlying local adaptation to environmental change.

In recent decades, research bridging the fields of molecular population genetics and quantitative genetics (Barghi et al., 2020; Barton, 1999; Pritchard et al., 2010; Pritchard & Di Rienzo, 2010) has revealed that the genomic architecture of a trait is a core determinant of whether and how that trait becomes locally adapted (Yeaman, 2022). Among the key aspects of genomic architecture that influence adaptation (Barton, 1999; Le Corre & Kremer, 2012; Yeaman, 2022; Yeaman & Whitlock, 2011) are the number of loci underlying a trait (henceforth, "polygenicity"), the rate of recombination between these loci (i.e., linkage), and the number of distinct genotypes that yield identical phenotypes (henceforth, "genotypic redundancy"). Previous research suggests that ecologically important traits can vary from having few loci of large effect (Martin & Orgogozo, 2013; Rees et al., 2020) to many loci of small effect (Barghi et al., 2020; Boyle et al., 2017; Rockman, 2012; Savolainen et al., 2013; Sella & Barton, 2019) and shows that variation in polygenicity can determine the rate and nature of local adaptation (Yeaman, 2015). Linkage controls the likelihood that adaptive alleles cluster together, essentially forming alleles of larger-effect size that are stronger targets of selection and more resistant to swamping gene flow (Yeaman & Whitlock, 2011), thereby facilitating local adaptation (Tigano & Friesen, 2016). Genotypic redundancy—a form of genetic redundancy that is defined as when more than one genotype can produce the same phenotype (Láruson et al., 2020)—can facilitate local adaptation by allowing the existence of a stable phenotypic cline governed by concerted shifts in underlying allele frequencies (Barghi et al., 2019; Manceau et al., 2010; Yeaman, 2015). We refer to this phenomenon as "transient genomic architecture."

The influence of genomic architecture on the nature and outcomes of local adaptation to changing environmental gradients has been studied to a limited extent, with a nearly exclusive focus on univariate models of the selective environment (but see Schiffers et al., 2013). These models have limitations for studying adaptation to climate change because, in nature, species can be adapted to multiple, independent environmental gradients (Guillaume, 2011) that can shift differentially, and thus decouple, as climate change advances (Daly et al., 2010; Crimmins et al., 2011), leading to the emergence of novel multivariate landscapes (Fitzpatrick et al., 2018; Williams et al., 2007; Williams & Jackson, 2007). Thus, it is important to investigate how the genomic architectures of multiple traits can combine to drive multivariate adaptation under climate change. Gene flow from "climate-suitable" portions of a species' range is often assumed to be beneficial for adaptation to climate change. This may be accurate from the perspective of a single trait adapted to a shifting climatic gradient, but it may be an invalid assumption if the gene flow also carries linked variation for a trait adapted to a second environmental variable from which the shifting gradient has decoupled. Under this scenario, gene flow may introduce alleles for the second trait that are disadvantageous and that could counteract any fitness advantage gained through the first trait. Thus, the genomic architectures of both traits may determine evolutionary outcomes by controlling the relative likelihoods of adaptation by gene flow and of in situ adaptation by shifting allelic covariance (Aitken & Whitlock, 2013; Schiffers et al., 2013).

Spatially explicit simulation is one of our strongest tools for improving our understanding of the complex dynamics of gene flow and adaptation under climate change (Capblancq et al., 2020). In this study, we use individual-based, spatially explicit simulations, constructed in `Geonomics` (Terasaki Hart et al., 2021), to test how genomic architecture influences multivariate adaptation to climate change. We simulate the adaptation of a single population continuously distributed on a two-dimensional landscape composed of two environmental variables, each structured as a gradient that runs parallel to the *x*-axis (Figure 1) and that exerts selection on a separate trait. In our main models, we then simulate climate change on that landscape by holding one gradient constant while gradually shifting the other gradient along the *x*-axis, such that the decoupling environment pushes local fitness peaks toward novel regions of two-dimensional trait space (Figure 1). We run 100 pairs of climate change simulations and null (stable-climate) simulations for each of 18 scenarios resulting from the full factorial crossing of three key components of genomic architecture: genotypic redundancy, polygenicity, and linkage (Table 1).

We analyze variation in the resulting spatiotemporal patterns of gene flow, population size and density, and phenotypic distributions—all of which are emergent properties of our simulation parameterizations (Code Sample S1)—to test a series of hypotheses about the influence of genomic architecture on multivariate adaptation under climate change. First, we hypothesize that up-gradient gene flow will be higher under climate change than under a stable climate across all scenarios, but that gene flow contributes least to climate change adaptation when linkage is low and polygenicity is high. This is because we expect gene flow to always have at least some adaptive value, but we also expect low-linkage, high-polygenicity architectures (i.e., "dispersed" architectures; Yeaman, 2022) to exhibit quick in situ adaptation via shifting allelic covariance among many small-effect alleles, facilitating phenotypic shifts in the absence of

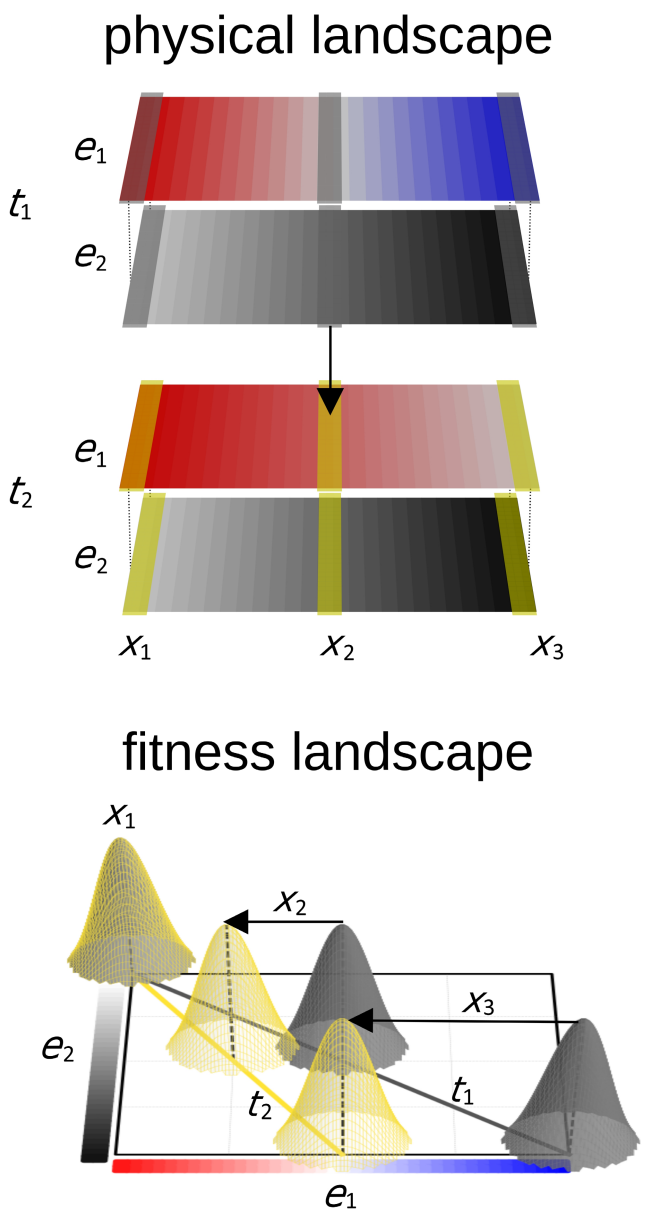

FIGURE 1 Conceptual model of adaptation to climate change. The top panel depicts the two-layered physical landscape used in our simulations, showing the shifting environmental gradient (e_1) in a blue–red color ramp and the stable gradient (e_2) in a white–black color ramp. The landscape is shown both before climate change (t_1) and after (t_2). The bottom panel depicts a fitness landscape for two traits adapted to the shifting (e_1) and stable gradients (e_2). Three example positions on the physical landscape (x_1, x_2, x_3) are shown as boxes delineated *y*-axis cross-sections, both before climate change (gray) and after (yellow), and their corresponding fitness peaks are shown as color-matched kernels on the fitness landscape. The gray and yellow lines on the fitness landscape indicate the fitness optima defined by the environments that exist before (t_1) and after climate change (t_2). Shifts in local fitness peaks are shown as labeled arrows (x_2, x_3); the environment at the far left of the physical landscape does not change, so x_1's fitness peaks are overlapping and have no shift.

up-gradient gene flow. Second, we hypothesize that stronger linkage and higher polygenicity will reduce a population's adaptive capacity under climate change, manifesting as greater reductions in population size and mean fitness and more persistent maladaptation, because both conditions impose longer expected wait times for the emergence of recombinant haplotypes that push phenotypes further from their pre-change fitness peaks. Finally, we hypothesize that higher genotypic redundancy will facilitate adaptation to shifting gradients, much as it does on stable gradients (Barghi et al., 2019; Manceau et al., 2010; Yeaman, 2015), resulting in smaller reductions in population size and mean fitness.

TABLE 1 Parameter values used for each of the three focal components of genomic architecture.

Component	Level	Parameter value
Genotypic redundancy	Low	`redund=1`
	High	`redund=2`
Polygenicity	Low	`n_loci=4 × redund`
	Mod	`n_loci=20 × redund`
	High	`n_loci=100 × redund`
Linkage	Low	`recomb=0.5`
	Mod	`recomb=0.05`
	High	`recomb=0.005`

Note: The full factorial combinations of these parameter values constitute the set of 18 simulation scenarios for which we present results.

2 | MATERIALS AND METHODS

2.1 | Simulations

We performed simulations using `Geonomics` v1.3.6 (Terasaki Hart et al., 2021), a Python (Van Rossum & Drake, 1995) package for forward-time, agent-based, continuous-space landscape genomic simulations. All of our simulated scenarios feature a species with two traits, each of which experiences selection on the basis of a different environmental variable. Both environmental variables are modeled as linear gradients running along the *x*-axis (Figure 1) that initially span environmental values from 1 to 0, left to right across the landscape. The genome is modeled as an array of length *L*, which in our two-trait simulations equals two times the number of genes per trait. Instead of randomly assigning loci to either of the two traits, we alternated locus trait assignment along the genome to avoid creating islands of within-trait linkage that would vary across iterations and introduce noise in our results. The fitness of individuals is a function of the difference between their local environmental values and their phenotypes, which are determined by the additive effects of multiple loci (i.e., without pleiotropy or epistasis), a reasonable approximation of many traits in real populations (Sella & Barton, 2019). Individuals have continuous spatial coordinates, and their local environmental values are found in the landscape cells within which their coordinates fall. Each time step has a movement phase during which each individual moves along a vector composed of a randomly drawn direction (from a uniform circular distribution) and a randomly drawn

distance [from a Wald (0.25, 0.5) distribution, such that most movements are less than one landscape cell in length].

Simulations start with a neutral burn-in period that does not include differential fitness. The burn-in is concluded when statistical tests of temporal and spatial population stability are passed, at which point individuals are randomly assigned genomes based on 0.5|0.5 allele frequencies at all loci. Simulations then run for 2500 time steps with differential fitness, generating a pattern of local adaptation to the initial environment. After that, one environmental layer undergoes a change event in which the gradient's values shift over a period of 250 time steps, resulting in a final gradient that spans values from 1 to 0.5, left to right. This creates a scenario in which the two environmental variables become decoupled, leading to the emergence of novel environments (i.e., sites occupying new values in two-dimensional environmental space), effectively modeling a common phenomenon under climate change (Fitzpatrick et al., 2018; Williams et al., 2007; Williams & Jackson, 2007). This generates spatially heterogeneous rates of climate change, ranging from no change at the leftmost edge to 0.002 units per time step at the rightmost edge. We chose this scenario because one with spatially homogeneous rates of change would generate an artifact of range expansion whose genomic signal could not reliably be disentangled from that of climate change adaptation. Hence, the approach we chose here allows us to isolate the evolutionary dynamics resulting from the components of genomic architecture that define our scenarios and hypotheses. The pre-climate change population sizes in our simulations varied around 5800–6100 individuals, which yields mean times to fixation of approximately 16,000–17,000 time steps (Terasaki Hart et al., 2021; Wright, 1931), roughly an order of magnitude larger than the total simulation length. Thus, the effects of drift during these simulations should be low, given the relatively large population sizes.

We used a custom Python script to set values for the parameters of interest in our simulations: the number of loci underlying each trait (parameter `n_loci`), the recombination rate between neighboring loci (parameter `recomb`), and the level of genotypic redundancy (parameter `redund`). The values we assigned to these parameters are provided in Table 1, and a visual depiction of the difference between low- and high-redundancy scenarios for all phenotypes is provided in Figure S1. We ran the simulations using Python v3.7 on the savio3 partition of UC Berkeley's Savio computing cluster (each node has 96 GB RAM and 32, 2.1-GHz Skylake processors). For each scenario, we ran a total of 100 iterations, featuring a 250 time step climate change period with natural selection (henceforth, the "main" scenarios), and 100 iterations of a paired null scenario without natural selection (henceforth, the "null" scenarios). We set all other `Geonomics` parameters to their default values. Some values of interest that might be explicit parameter settings in other simulation programs are instead emergent properties in `Geonomics`; for example, the population size values we report emerge from the interaction of several explicit parameters, including the raster of local carrying capacities, the population intrinsic growth rate, the number of offspring per reproduction event, and the death rates resulting from the parameters controlling density-dependent mortality and natural selection. The complete set of `Geonomics` parameters and the values we assigned to them across all models are provided in Code Sample S1. The parameters we set correspond best to a scenario of a moderately mobile species with occasional longer-distance dispersal, overlapping generations, and repeat reproduction of small numbers of offspring.

Using a combination of internal `Geonomics` functions and custom Python code, we designed a set of data outputs from each model run to visualize results and test hypotheses. We saved tables of the locations and phenotypes for all individuals at the beginning and end of the climate change period. We also saved time series of population size, mean fitness, and the mean phenotype of the trait adapted to the shifting gradient. We gathered this data at every time step for the 250 time steps immediately before the onset of climate change, 250 time steps during the climate change period, and 250 time steps after climate change completed (hereafter, the "post-change period").

We also saved data on the vector directions of gene flow occurring during climate change by keeping data for two randomly chosen loci underlying the trait adapted to the shifting environmental gradient (with positive effect) for all of the individuals remaining in the final time step. Capturing loci expected to facilitate adaptation to increasing environmental values allowed us to track up-gradient gene flow, and it provided equal sample sizes across scenarios for downstream analysis (which was constrained to the number of positive-effect loci in the low-polygenicity, low-redundancy scenarios). We collected these data using an internal function that extracts data from the spatial pedigrees stored in the simulation's `tskit` (Kelleher et al., 2018) data structures. We also calculated a single summary metric of "up-gradient gene flow" for each iteration:

$$\mathrm{GF}_{\mathrm{up}} = \frac{\sum_i^n \cos\theta}{n}, \cos\theta \geq 0,$$

where θ is the angle of gene flow, expressed counterclockwise from the right. The $\cos\theta \geq 0$ condition allowed us to track only rightward (up-gradient) gene flow and to omit leftward (down-gradient) gene flow, which would be maladaptive for the positive-effect loci we tracked and, thus, low irrespective of scenario.

2.2 | Analysis

We analyzed the results of our simulations using custom scripts written in Python v3.7 (Van Rossum & Drake, 1995) and R v4.0 (R Core Team, 2021). To test our first hypothesis—that up-gradient gene flow should be greater under climate change scenarios—we first produced a visualization of the directional distributions of gene flow under all 18 scenarios, comparing between main and null simulations (Figure 2) based on the random sample of the gene flow that occurred during the climate change period that we captured from our simulations. We then fitted a mixture of four von Mises distributions to that data using the R package `movMF` v0.2-6 (Hornik & Grün, 2014), yielding 12 parameter estimates defining each simulation's fitted mixture distribution. For each of the 18 scenarios, we then plotted the probability

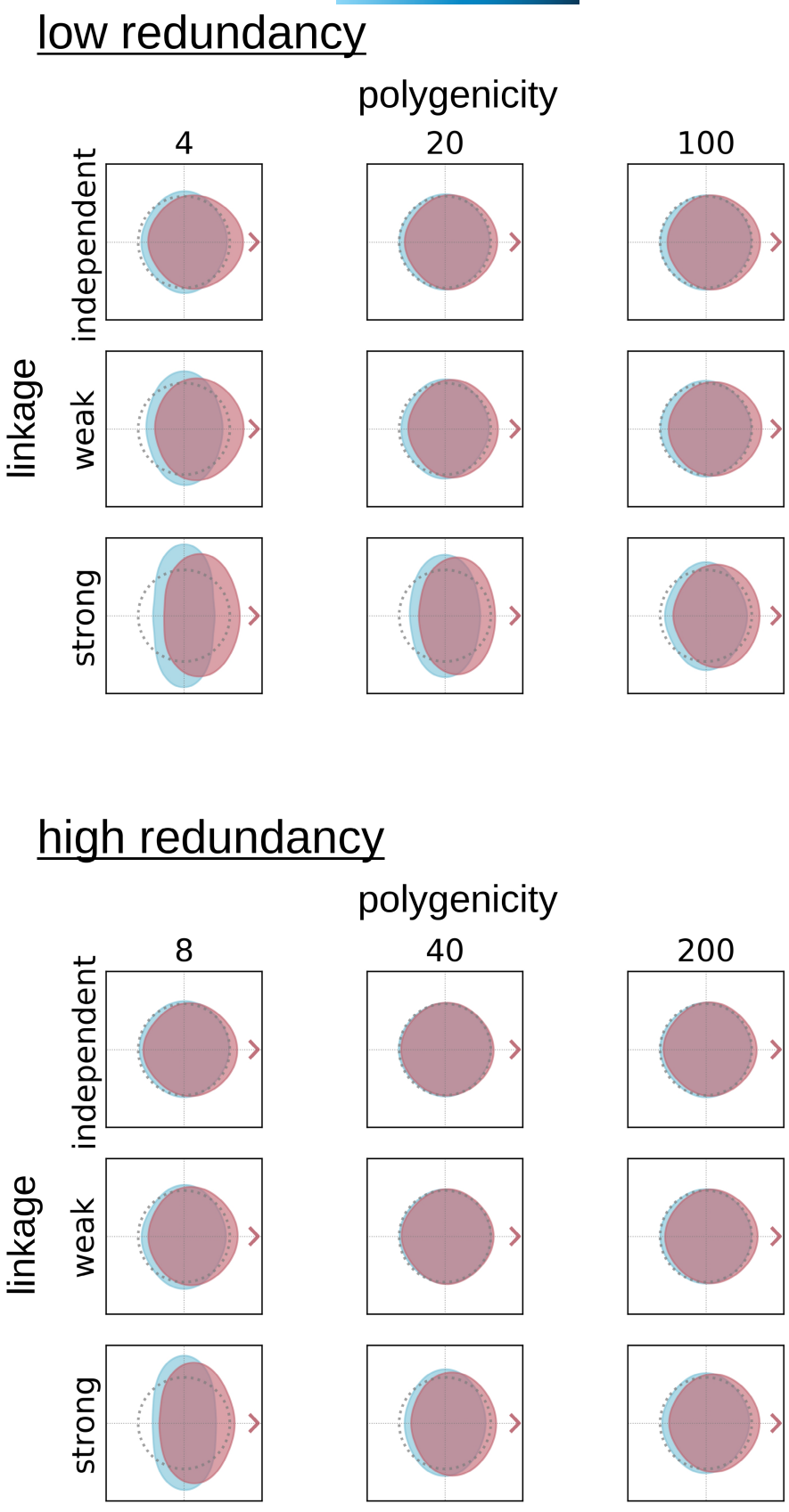

FIGURE 2 Distributions of gene flow directions during the climate change period of our climate change simulations (red) compared to null simulations (blue) for our 18 scenarios. The shifting environmental gradient moves to the right (in the direction of the arrow) in our simulations, so rightward gene flow represents up-gradient gene flow, and upward and downward (i.e., "on contour") gene flow is perpendicular to the environmental gradients. Down-gradient gene flow is expected to be maladaptive under all scenarios, explaining why it is universally suppressed relative to the null results (as evidenced by the blue distributional "margins" extending to the left of the red distributions in all scenarios). There is a general trend toward increasing on-contour gene flow and decreasing up-gradient gene flow, with decreasing linkage and increasing polygenicity.

density function described by the means of all vectors of fitted parameters. We did this separately for null scenarios and for main scenarios, then overlaid the results for the main scenarios (in red) on top of the null results (in blue; Figure 2), providing a visualization of the directionality of gene flow within each climate change scenario compared to its null expectation.

We also ran a simple linear regression of the main versus null difference in up-gradient gene flow density as a function of polygenicity, linkage, and redundancy. We coded the genomic architecture components as integer variables representing the levels of the parameter values used in the simulations (redundancy: low = 1, high = 2; polygenicity: low = 0, moderate = 1, high = 2; linkage: low = 0, moderate = 1, high = 2). We used the regression results to test both predictions for our first hypothesis: (1) that the main − null difference in up-gradient gene flow should have 95% confidence intervals >0 under all scenarios (calculated using the `stats` package's `predict.lm` function with the argument `interval = "confidence"`), indicating significant up-gradient gene flow under climate change; and (2) that the coefficients for the linkage (β_l) and polygenicity (β_p) terms of the model should be significantly positive and negative, respectively, indicating that higher levels of gene flow are associated with stronger linkage and lower polygenicity.

To visually assess our second and third hypotheses, we created a series of plots comparing climate change-driven demographic shifts and maladaptation across all 18 scenarios and between our null and main models. First, we plotted the null and main time series of two demographic metrics, mean fitness and population size, for each of our 18 scenarios, combining the results for all 100 iterations under each scenario. For each time series, we calculated the mean and the 5th and 95th percentiles at each time step (Figure 3; Figure S2). We also summarized all scenarios in a pair of box plots (Figure S2).

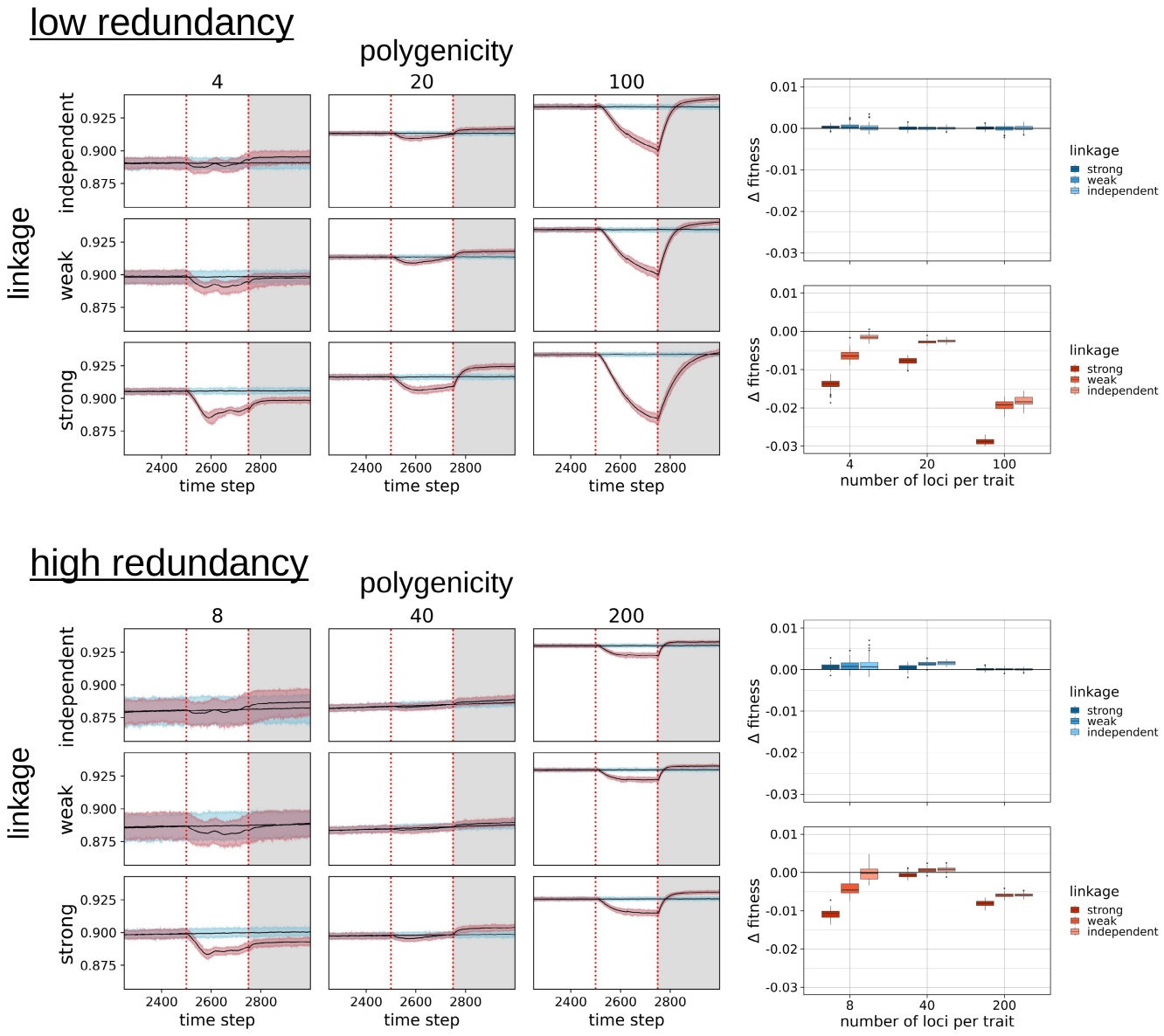

FIGURE 3 Left: Mean fitness for all scenarios during the 250 time steps before, during, and after the climate change period (separated by red, dashed lines). Black lines represent the mean values, and the shaded red and blue areas represent variability envelopes (5th percentile to 95th percentile) for all replicates for climate change and null simulations, respectively. Right: Boxplots of changes in mean fitness during the climate change period for all scenarios. Null scenarios are plotted on the top in blue, and main scenarios are plotted on the bottom in red. Within each plot, the scenarios are organized by polygenicity (number of loci per trait) on the *x*-axis and shaded by the strength of linkage.

To better understand changes in population size and distribution, we also mapped before and after comparisons of population densities for all 18 main scenarios (Figure S3). Each population density map was calculated as the mean population density at each cell on the landscape, averaged across all 100 iterations.

Finally, to visualize maladaptation, we plotted each scenario's mean phenotypic distributions before and after climate change as scatter plots of the density of individuals occurring across two-dimensional trait space. We plotted lines and wedges depicting the average maladaptation observed across each scenario's 100 iterations (Figure 4). We refer to the wedge as "persistent maladaptation," and we calculated it as the difference between: (a) the area within two-dimensional trait space that the population's phenotypic distribution would have needed to shift through during the climate change event to remain optimally fit to its environment, and (b) the observed area of phenotypic shift within a scenario's 100 simulations. We qualify this metric as "persistent" to emphasize that it does not reflect transient maladaptation that arises but then resides during the period of climate change but rather reflects only maladaptation that remained at the end of the climate change period. To measure this area, we first determined the triangular area between the expected central tendency lines of the optimal two-dimensional phenotypic distributions before and after the climate change event. Then, for each model run, we used ordinary least squares to fit a central tendency line to the 100-iteration ensemble phenotypic distribution observed at the end of the climate change event [fixing the *y*-intercept at the (1, 1) point in phenotypic space, which represents the unchanging phenotypic optimum at the left-most extent of the landscape]. The area of the wedge between the expected and observed post-change central tendency lines provides our measure of a scenario's persistent maladaptation. We plotted before and after scatter plots of the ensemble datasets of individuals' two-dimensional phenotypes (binned to a grid of regular points for interpretability). We also produced these plots (Figure S4) using data from our null simulations to demonstrate that all differences in maladaptation observed between scenarios were attributable to climate change.

To statistically evaluate our results, we ran simple linear regressions for each of our three response variables measuring population-level changes during the climate change event—change in mean fitness, change in population size, and persistent maladaptation—with polygenicity, linkage, redundancy, and nullness serving as explanatory variables. We modeled nullness as a binary categorical variable (null = 0, main = 1) and again modeled the genomic architecture components as integer variables, as described above. We used these regressions to test our second (polygenicity and linkage) and third (redundancy) hypotheses. Specifically, our second hypothesis predicts that the coefficients of the linkage and polygenicity terms are significantly non-zero and negative (for changes in fitness change and population size) and positive (for the maladaptation model), while our third hypothesis predicts significantly non-zero redundancy coefficients with the opposite signs.

3 | RESULTS

3.1 | Gene flow

Under our simulations, climate change led to a nearly universal increase in up-gradient gene flow compared to null simulations with no change to either environmental variable. For all 18 of our simulated scenarios (Figure 2), the simulations with climate change exhibited greater up-gradient gene flow than the null scenarios, and linear regressions modeling the effects of linkage, redundancy, and polygenicity on up-gradient gene flow found that the fitted 95% confidence intervals for up-gradient gene flow were >0 for all but one scenario (the moderate-polygenicity, low-linkage, high-redundancy scenario; Table S1). However, the magnitude of this increase in gene flow was minimal under some scenarios. We found that the difference in up-gradient gene flow between climate change and null simulations was positively correlated with linkage ($\beta_l = 0.0129 \pm 0.0006$, $p < 1 \times 10^{-15}$) and inversely correlated with polygenicity ($\beta_l = 0.0142 \pm 0.0006$, $p < 1 \times 10^{-15}$), corroborating our first hypothesis. Correspondingly, and in line with expectations, down-gradient gene flow was universally suppressed under climate change (Figure 2). Of the three components of genomic architecture that we tested, polygenicity had the most striking effect on the extent to which up-gradient gene flow contributed to adaptation; moderate- and high-polygenicity scenarios generally had much lower up-gradient gene flow than did low-polygenicity scenarios, with low-redundancy, independent-linkage scenarios being the main exception (Figure 2). Moderate-polygenicity scenarios actually showed the lowest overall increase in up-gradient gene flow, though differences between moderate- and high-redundancy scenarios were minor.

3.2 | Linkage and polygenicity

As expected, our null simulations showed essentially no changes in mean fitness (Figure 2) or population size (Figure S2), aside from small modeling artifacts present in both the null and climate change scenarios, and the phenotypic distributions for the populations in these simulations were stable through time (Figure S4). The results of our climate change simulations exhibited decreases in population size and mean fitness that are the expected results of increasing maladaptation (Aitken & Whitlock, 2013). They also revealed environment-tracking phenotypic shifts (Figure 4) in line with expectations (Figure 1), though these shifts lagged behind environmental change to some extent, producing suboptimal mean fitness at the end of the climate change period. Across scenarios, the demographic responses to climate change, in terms of population size and fitness, increased with increasing linkage (change in fitness: $\beta_l = 0.0018 \pm 0.0001$, $p < 1 \times 10^{-15}$; change in population size: $\beta_l = 33.330 \pm 1.287$, $p < 1 \times 10^{-15}$). We also found greater maladaptation, defined as the area in two-dimensional trait space separating the central line of a population's post-change phenotypic

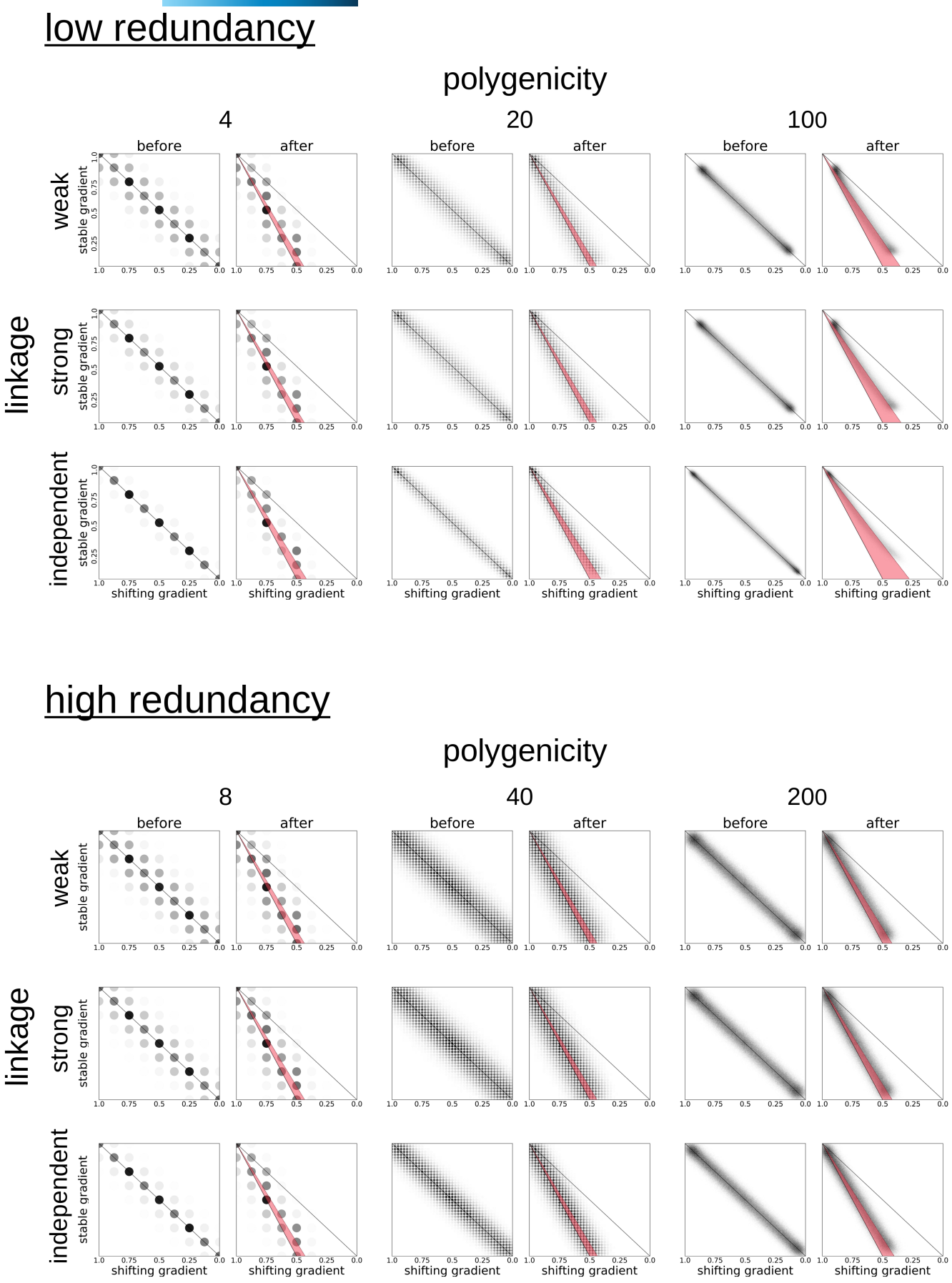

FIGURE 4 Scatterplots of the observed versus expected phenotypic shift during the climate change period for all 18 of our simulated scenarios. For each scenario, the left ("before") scatterplot shows the distribution of phenotypes before climate change begins, and the right ("after") scatterplot shows how the distribution has shifted by the end of the climate change period. The trait adapted to the shifting environmental gradient is distributed along the *x*-axis, with the trait adapted to the stable gradient on the *y*-axis. Each plot is an ensemble of the results for all 100 replicates of each scenario. The size and opacity of each point represent the number of individuals exhibiting that two-dimensional phenotype. The gridded arrangement of the points in each scatterplot is a function of the number of loci per trait, which determines the set of possible phenotypes. Solid black lines delineate the shifts in the phenotypic distributions' central tendencies that are expected to take place during the climate change period; dotted black lines depict the observed distributions' central tendencies; and red wedges depict the differences between the expected and observed distributions ("phenotypic shortfall").

distribution from the central line of the distribution that would optimally track the changing environment (Figure 4; Figure S4), associated with increasing linkage (maladaptation: $\beta_l = 0.0038 \pm 0.0004$, $p < 1 \times 10^{-15}$).

The magnitude of demographic responses also showed a signal of an overall increase with increasing polygenicity (change in fitness: $\beta_p = 0.0022 \pm 0.0001$, $p < 1 \times 10^{-15}$; change in population size: $\beta_p = 15.070 \pm 1.287$, $p < 1 \times 10^{-15}$; maladaptation: $\beta_p = 0.0097 \pm 0.0004$, $p < 1 \times 10^{-15}$), although the trend was non-monotonic and complex. Responses were smallest at moderate polygenicity, more pronounced at low polygenicity, and highest at high polygenicity and low redundancy (Figure 3; Figure S2). In fact, under high polygenicity and low redundancy, populations declined so strongly that adaptive capacity was effectively outstripped, and the declines persisted throughout the climate change period, with little indication of evolutionary rescue (i.e., stabilization and rebound) occurring until the post-change period (Figure 3; Figure S2). The collapse of adaptive capacity in these scenarios is also visible in the large areas of phenotypic-shift shortfall in Figure 4. The low-redundancy, high-polygenicity, strong-linkage scenario had such low adaptive capacity that mean fitness declined by 5.2% on average (from 0.934 to 0.885), mean population size declined by 17.1% on average (from 6326 to 5246 individuals), and the simulated population ceased to occupy the rightmost, fastest-changing portion of the landscape (Figure 4).

3.3 | Genotypic redundancy

Our high-redundancy scenarios showed consistently smaller demographic responses to climate change, less-prominent up-gradient gene flow, and higher adaptive capacity than their low-redundancy counterparts (change in fitness: $\beta_r = 0.0040 \pm 0.0002$, $p < 1 \times 10^{-15}$; change in population size: $\beta_r = 39.060 \pm 2.101$, $p < 1 \times 10^{-15}$; maladaptation: $\beta_r = 0.0098 \pm 0.0006$, $p < 1 \times 10^{-15}$), consistent with our hypothesis that genotypic redundancy can facilitate adaptation to shifting environmental gradients (Figure 2; Figure S2). This effect was most pronounced in the high-polygenicity scenarios, which exhibited much milder demographic decline under high redundancy compared to low redundancy, despite still showing no evidence of demographic rebound until after climate change (Figure 3). Indeed, increased redundancy puts the demographic declines under these scenarios on par with those of the low-polygenicity scenarios (Figure 3; Figure S2).

4 | DISCUSSION

Current theoretical understanding of evolutionary responses to climate change largely derives from a simplified mechanistic model in which adaptation is universally facilitated by up-gradient gene flow. This model also serves as the inspiration for some climate-smart approaches to biodiversity management (e.g., assisted gene flow; Aitken & Whitlock, 2013). However, adopting this model as the basis for theoretical and mechanistic research risks overlooking the influence of genomic architecture on multivariate adaptation to environmental change. Starting from a more realistic, multi-trait framework, our simulations demonstrate that up-gradient gene flow does indeed occur under climate change but that its contributions to local adaptation and persistence may be constrained by polygenicity, genotypic redundancy, and, to a lesser extent, linkage. Given the range of plausible genomic architectures we simulate (Barghi et al., 2020; Bomblies & Peichel, 2022; Boyle et al., 2017; Rockman, 2012; Savolainen et al., 2013; Sella & Barton, 2019), these results raise the compelling possibility that up-gradient gene flow, while unlikely to be entirely maladaptive, could play a limited role in climate change adaptation in many systems. This may be especially true in systems where climate-adapted traits have more dispersed architectures—for example, architectures composed of many genes of small effect (Yeaman, 2022). This poses an important question for subsequent research: how often are the genomic architectures underlying climate-adapted traits dispersed versus concentrated?

We also show that the genomic architecture of climate-adapted traits can influence the nature and size of demographic responses to climate change. Our results suggest that strong linkage between non-neutral loci, especially under high polygenicity, can increase maladaptation and demographic decline during climate change. In the most extreme case, evolutionary rescue was absent; high polygenicity and low redundancy combined to drive dramatic and persistent demographic declines and even caused local extinction when linkage was strong. This was unexpected in light of previous work reporting that dispersed architectures produce stable, resilient phenotypic clines despite transient genotypic composition (Yeaman, 2015, 2022) and, thus, that species with such architectures could exhibit rapid local adaptation (Aitken et al., 2008). We did, nonetheless, expect evolutionary responses to climate change to be slower in these scenarios, because natural selection is less effective on smaller-effect alleles, gene flow may have more of a swamping effect for these alleles, and high linkage leads to longer expected wait times for the generation of novel, adaptive recombinant genotypes. We did not, however, expect adaptive capacity to be completely outstripped. Yet, it appears that the rate of environmental change simply exceeded the

pace of adaptation. This is evidenced by the quick demographic rebound that occurred in the "post-change" periods (Figure 3). This rebound was likely driven by the same evolutionary dynamics that occur during evolutionary rescue, but in these extreme scenarios, it only emerged once environmental change had ceased.

Remarkably, we also observed higher maladaptation and larger demographic declines in our low-polygenicity scenarios with fewer, larger-effect alleles. Demographic decline was least pronounced in our moderate-polygenicity models. This contrasts with previous work finding that adaptation to a gradient is more effective under either concentrated or dispersed genomic architectures (Yeaman & Whitlock, 2011). This disagreement may be attributable to the difference in timeframes between adaptation to a univariate environmental gradient and adaptation to a decoupled, multivariate gradient. Adaptation to a single, static gradient can proceed gradually, which may favor large-effect alleles or allele clusters over longer time scales, once they have arisen by mutation, recombination, gene flow, or a combination thereof (Yeaman, 2015, 2022). Longer-term, gradual change scenarios may also favor dispersed architectures in temporally fluctuating environments (Bürger & Gimelfarb, 2002; Kondrashov & Yampolsky, 1996; Yeaman, 2022; Yeaman & Whitlock, 2011). However, the sudden onset of persistent environmental change in a population that is already locally adapted triggers a "race against time," and genomic architectures with optimal adaptive capacity may be the "middle ground" architectures that comprise freely recombining loci with small enough effect sizes to avoid large declines in fitness from migration load but with large enough effect sizes to allow for effective natural selection and to avoid the long wait times necessary for recombination to cluster many adaptive loci into larger-effect haplotypes. This presents the surprising possibility that an "evolutionary trade-off" may exist, such that mid-effect-size alleles may confer maximal adaptive capacity to environmental change.

The fact that high genotypic redundancy reduces demographic decline, across all scenarios, contributes to the growing recognition of the importance of redundancy as a driver of evolutionary outcomes for polygenic traits (Láruson et al., 2020; Yeaman, 2022). This also presents a possible mechanism to be explored in real-world populations living at colder range edges. Much like the local populations in the rightmost region of our low-redundancy scenarios, these local populations could already be at the edge of the phenotypic space defined by their standing genetic variation. In this case, segregating redundancy (Láruson et al., 2020) and, thus, adaptive capacity would be low, so vulnerability to local extinction would be substantial. However, species whose cold range edges are predominantly determined by geographic barriers or biotic interactions rather than climate limits (Thomas, 2010) could feature local populations more similar to our high-redundancy scenarios; segregating redundancy would be higher, so selection would be balancing rather than directional, and adaptive capacity would be substantial. Hence, in situ adaptation would be a substantial contributor to adaptive capacity in these scenarios—an implication supported by the fact that we observed reduced upgradient gene flow across all high-redundancy scenarios.

Our findings also contribute new insight to the theoretical understanding of local adaptation with recombination. Recombination is generally regarded as disadvantageous in situations of clinal adaptation with gene flow, because it disrupts the association between adaptive loci underlying a single trait (Tigano & Friesen, 2016). Unstable environments experiencing stochastic temporal fluctuations are considered a major exception (Tigano & Friesen, 2016), but our results suggest that this may also extend to environments undergoing monotonic change such as that caused by climate change. In fact, recombination may be advantageous under these conditions, particularly when species have distinct traits simultaneously adapted to decoupled environmental gradients. This advantage likely arises because recombination allows for more effective in situ adaptation by shifting allelic covariance, despite still disrupting the associations between loci that would otherwise allow for the development of larger-effect gene clusters. This suggests that in situ shifts in allelic covariance provide an alternative to adaptive gene flow as a mechanism for evolutionary rescue, especially in multi-trait systems where gene flow can be adaptive for shifting climatic gradients but maladaptive with respect to other, decoupled gradients.

A major challenge in simulation-based research is the complexity of the high-dimensional parameter space that could be explored. Useful and informative studies can be constructed by focusing on a small set of key parameters while holding others at reasonable values, as we have done here. This nonetheless leaves unexplored a number of secondary parameters that can have a non-negligible influence over the complex ecological phenomena of interest. In the case of evolutionary responses to climate change, this provides various areas for future research. These include population size, a major determinant of the relative strengths of drift and natural selection (Murray et al., 2017) and of the wait time to emergence of recombinant haplotypes (Christiansen et al., 1998); movement behavior, a key factor influencing migration–selection dynamics (Barton, 1999; Haldane, 1930; Wright, 1931); allelic effect size distributions (Orr, 1998), which are omitted here in favor of a single, fixed effect size; and the spatiotemporal structure of the environment, including gradient geometries, slopes, orientations, and rates of change (Benes & Bracken, 2020). Additionally, important and conservation-relevant insight could emerge from the integration of other dimensions of climate change ecology, including range shifts (Weiss-Lehman & Shaw, 2020), plasticity (Chevin et al., 2010), and range-wide variation in population densities (Aitken & Whitlock, 2013). Finally, more complex evolutionary scenarios could also be explored, including pleiotropy and epistasis (Thompson, 2020), hybridization (Turbek & Taylor, 2023), life history variation, and even multiple traits that differ in the complexity of their genomic architectures—a realistic scenario that could exhibit different evolutionary outcomes than the ones we describe here.

5 | CONCLUSIONS

Adaptive gene flow and in situ adaptation are two of the main processes by which species may persist under climate change. Evaluating the conditions under which they are likely to contribute to species persistence is essential for better understanding

microevolutionary responses to climate change and for informing management efforts. Our simulations show that genomic architecture can play an important, but largely overlooked, role in driving evolutionary outcomes. This includes determining the relative effectiveness of these two processes, the magnitude and persistence of maladaptation, and the likelihood of concomitant demographic decline or evolutionary rescue. These findings highlight the importance of considering multivariate environmental gradients for climate change research, and suggest that the genomic architecture underlying traits adapted to those gradients has direct consequences for how species respond to environmental change.

AUTHOR CONTRIBUTIONS

Drew E. Terasaki Hart: Conceptualization; data curation; formal analysis; funding acquisition; investigation; methodology; project administration; resources; software; validation; visualization; writing – original draft; writing – review and editing. **Ian J. Wang:** Conceptualization; funding acquisition; methodology; project administration; supervision; writing – review and editing.

ACKNOWLEDGMENTS

We thank A.P. Bishop, T. Dawson, J. Frederick, N. Graham, M. Kelly, M. McElroy, E. Westeen, G. Wogan, and M. Yuan for feedback and guidance on various iterations of the simulations presented herein. We thank Berkeley Research Computing for providing access to the Savio computing cluster. We thank D. Ehrenfeld, N. Fefferman, M. Fitzpatrick, and L. Plough for cultivating an interest in conservation genetics. Lastly, we thank M. Terasaki Hart, C.A. Nemec-Hart, G.B. Hart, J. Hart, and M. Tylka for supporting and encouraging a lifetime of curiosity about nature, and C. Adjuah, B. Evans, R. Pérez Joglar, Y.Y. Ma, and J. Redman for the great company during long periods of solitude. This work was supported by a Berkeley Fellowship from the University of California, Berkeley (to D.E.T.H.), by a Bezos Earth Fund grant to The Nature Conservancy (which covered some time for D.E.T.H.), and by National Science Foundation grant DEB1845682 (to I.J.W.).

CONFLICT OF INTEREST STATEMENT

The authors claim no conflicts of interest.

DATA AVAILABILITY STATEMENT

All data used to derive the results presented herein are publicly available in Zenodo at http://doi.org/10.5281/zenodo.10547538. Code is publicly available on GitHub at http://github.com/erthward/climate_change_adaptation_and_genomic_arch (http://doi.org/10.5281/zenodo.10531208).

ORCID

Drew E. Terasaki Hart https://orcid.org/0000-0003-1832-2289

REFERENCES

Ackerly, D. D., Loarie, S. R., Cornwell, W. K., Weiss, S. B., Hamilton, H., Branciforte, R., & Kraft, N. J. B. (2010). The geography of climate change: Implications for conservation biogeography. *Diversity and Distributions*, *16*(3), 476–487.

Aitken, S. N., & Whitlock, M. C. (2013). Assisted gene flow to facilitate local adaptation to climate change. *Annual Review of Ecology, Evolution, and Systematics*, *44*(1), 367–388.

Aitken, S. N., Yeaman, S., Holliday, J. A., Wang, T., & Curtis-McLane, S. (2008). Adaptation, migration or extirpation: Climate change outcomes for tree populations. *Evolutionary Applications*, *1*(1), 95–111.

Barghi, N., Hermisson, J., & Schlötterer, C. (2020). Polygenic adaptation: A unifying framework to understand positive selection. *Nature Reviews Genetics*, *21*(12), 769–781.

Barghi, N., Tobler, R., Nolte, V., Jakšić, A. M., Mallard, F., Otte, K. A., Dolezal, M., Taus, T., Kofler, R., & Schlötterer, C. (2019). Genetic redundancy fuels polygenic adaptation in *Drosophila*. *PLoS Biology*, *17*(2), e3000128.

Barton, N. H. (1999). Clines in polygenic traits. *Genetics Research*, *74*(3), 223–236.

Bell, G., & Gonzalez, A. (2011). Adaptation and evolutionary rescue in metapopulations experiencing environmental deterioration. *Science*, *332*(6035), 1327–1330.

Bellis, J., Bourke, D., Maschinski, J., Heineman, K., & Dalrymple, S. (2020). Climate suitability as a predictor of conservation translocation failure. *Conservation Biology*, *34*(6), 13518. https://doi.org/10.1111/cobi.13518

Benes, K. M., & Bracken, M. E. S. (2020). Interactive effects of large- and local-scale environment gradients on phenotypic differentiation. *Ecology*, *101*(8), e03078. https://doi.org/10.1002/ecy.3078

Bomblies, K., & Peichel, C. L. (2022). Genetics of adaptation. *Proceedings of the National Academy of Sciences of the United States of America*, *119*(30), e2122152119.

Boyle, E. A., Li, Y. I., & Pritchard, J. K. (2017). An expanded view of complex traits: From polygenic to omnigenic. *Cell*, *169*(7), 1177–1186.

Bürger, R., & Gimelfarb, A. (2002). Fluctuating environments and the role of mutation in maintaining quantitative genetic variation. *Genetics Research*, *80*(1), 31–46.

Capblancq, T., Fitzpatrick, M. C., Bay, R. A., Exposito-Alonso, M., & Keller, S. R. (2020). Genomic prediction of (mal)adaptation across current and future climatic landscapes. *Annual Review of Ecology, Evolution, and Systematics*, *51*(1), 1–25.

Chevin, L.-M., Lande, R., & Mace, G. M. (2010). Adaptation, plasticity, and extinction in a changing environment: Towards a predictive theory. *PLoS Biology*, *8*(4), e1000357.

Christiansen, F. B., Otto, S. P., Bergman, A., & Feldman, M. W. (1998). Waiting with and without recombination: The time to production of a double mutant. *Theoretical Population Biology*, *53*(3), 199–215.

Crimmins, S. M., Dobrowski, S. Z., Greenberg, J. A., Abatzoglou, J. T., & Mynsberge, A. R. (2011). Changes in climatic water balance drive downhill shifts in plant species' optimum elevations. *Science*, *331*(6015), 324–327.

Daly, C., Conklin, D. R., & Unsworth, M. H. (2010). Local atmospheric decoupling in complex topography alters climate change impacts. *International Journal of Climatology*, *30*(12), 1857–1864.

Feder, J. L., Gejji, R., Yeaman, S., & Nosil, P. (2012). Establishment of new mutations under divergence and genome hitchhiking. *Philosophical Transactions of the Royal Society, B: Biological Sciences*, *367*(1587), 461–474.

Felsenstein, J. (1976). The theoretical population genetics of variable selection and migration. *Annual Review of Genetics*, *10*(1), 253–280.

Fitzpatrick, M. C., Blois, J. L., Williams, J. W., Nieto-Lugilde, D., Maguire, K. C., & Lorenz, D. J. (2018). How will climate novelty influence ecological forecasts? Using the quaternary to assess future reliability. *Global Change Biology*, *24*(8), 3575–3586. ISSN 1354-1013.

Guillaume, F. (2011). Migration-induced phenotypic divergence: The migration–selection balance of correlated traits. *Evolution: International Journal of Organic Evolution*, *65*(6), 1723–1738.

Haldane, J. B. S. (1930). A mathematical theory of natural and artificial selection (part VI, isolation). In *Mathematical Proceedings of the Cambridge Philosophical Society* (Vol. *26*, pp. 220–230). Cambridge University Press.

Harrisson, K. A., Pavlova, A., Telonis-Scott, M., & Sunnucks, P. (2014). Using genomics to characterize evolutionary potential for conservation of wild populations. *Evolutionary Applications*, *7*(9), 1008–1025.

Hornik, K., & Grün, B. (2014). movMF: An R package for fitting mixtures of Von Mises-Fisher distributions. *Journal of Statistical Software*, *58*(10), 1–31.

Kelleher, J., Thornton, K. R., Ashander, J., & Ralph, P. L. (2018). Efficient pedigree recording for fast population genetics simulation. *PLoS Computational Biology*, *14*(11), e1006581. https://doi.org/10.1371/journal.pcbi.1006581

Kondrashov, A. S., & Yampolsky, L. Y. (1996). High genetic variability under the balance between symmetric mutation and fluctuating stabilizing selection. *Genetics Research*, *68*(2), 157–164.

Láruson, Á. J., Yeaman, S., & Lotterhos, K. E. (2020). The importance of genetic redundancy in evolution. *Trends in Ecology & Evolution*, *35*(9), 809–822.

Le Corre, V., & Kremer, A. (2012). The genetic differentiation at quantitative trait loci under local adaptation. *Molecular Ecology*, *21*(7), 1548–1566.

Lenormand, T. (2002). Gene flow and the limits to natural selection. *Trends in Ecology & Evolution*, *17*(4), 183–189.

Loarie, S. R., Duffy, P. B., Hamilton, H., Asner, G. P., Field, C. B., & Ackerly, D. D. (2009). The velocity of climate change. *Nature*, *462*(7276), 1052–1055.

Manceau, M., Domingues, V. S., Linnen, C. R., Rosenblum, E. B., & Hoekstra, H. E. (2010). Convergence in pigmentation at multiple levels: Mutations, genes and function. *Philosophical Transactions of the Royal Society, B: Biological Sciences*, *365*(1552), 2439–2450.

Martin, A., & Orgogozo, V. (2013). The loci of repeated evolution: A catalog of genetic hotspots of phenotypic variation. *Evolution*, *67*(5), 1235–1250.

Murray, G. G. R., Soares, A. E. R., Novak, B. J., Schaefer, N. K., Cahill, J. A., Baker, A. J., Demboski, J. R., Doll, A., Da Fonseca, R. R., Fulton, T. L., Gilbert, M. T. P., Heintzman, P. D., Letts, B., McIntosh, G., O'Connell, B. L., Peck, M., Pipes, M. L., Rice, E. S., Santos, K. M., … Shapiro, B. (2017). Natural selection shaped the rise and fall of passenger pigeon genomic diversity. *Science*, *358*(6365), 951–954.

Nicotra, A. B., Beever, E. A., Robertson, A. L., Hofmann, G. E., & O'Leary, J. (2015). Assessing the components of adaptive capacity to improve conservation and management efforts under global change. *Conservation Biology*, *29*(5), 1268–1278.

Orr, H. A. (1998). The population genetics of adaptation: The distribution of factors fixed during adaptive evolution. *Evolution*, *52*(4), 935–949.

Pritchard, J. K., & Di Rienzo, A. (2010). Adaptation–not by sweeps alone. *Nature Reviews Genetics*, *11*(10), 665–667.

Pritchard, J. K., Pickrell, J. K., & Coop, G. (2010). The genetics of human adaptation: Hard sweeps, soft sweeps, and polygenic adaptation. *Current Biology*, *20*(4), R208–R215.

R Core Team. (2021). *R: A language and environment for statistical computing*. R Foundation for Statistical Computing. https://www.R-project.org/

Rees, J. S., Castellano, S., & Andrés, A. M. (2020). The genomics of human local adaptation. *Trends in Genetics*, *36*(6), 415–428.

Rockman, M. V. (2012). The qtn program and the alleles that matter for evolution: All that's gold does not glitter. *Evolution: International Journal of Organic Evolution*, *66*(1), 1–17.

Savolainen, O., Lascoux, M., & Merilä, J. (2013). Ecological genomics of local adaptation. *Nature Reviews Genetics*, *14*(11), 807–820.

Schiffers, K., Bourne, E. C., Lavergne, S., Thuiller, W., & Travis, J. M. J. (2013). Limited evolutionary rescue of locally adapted populations facing climate change. *Philosophical Transactions of the Royal Society, B: Biological Sciences*, *368*(1610), 20120083.

Sella, G., & Barton, N. H. (2019). Thinking about the evolution of complex traits in the era of genome-wide association studies. *Annual Review of Genomics and Human Genetics*, *20*, 461–493.

Slatkin, M. (1987). Gene flow and the geographic structure of natural populations. *Science*, *236*(4803), 787–792.

Terasaki Hart, D. E., Bishop, A. P., & Wang, I. J. (2021). Geonomics: Forward-time, spatially explicit, and arbitrarily complex landscape genomic simulations. *Molecular Biology and Evolution*, *38*(10), 4634–4646.

Thomas, C. D. (2010). Climate, climate change and range boundaries. *Diversity and Distributions*, *16*(3), 488–495.

Thompson, K. A. (2020). Experimental hybridization studies suggest that pleiotropic alleles commonly underlie adaptive divergence between natural populations. *The American Naturalist*, *196*(1), E16–E22. https://doi.org/10.1086/708722

Tigano, A., & Friesen, V. L. (2016). Genomics of local adaptation with gene flow. *Molecular Ecology*, *25*(10), 2144–2164.

Turbek, S. P., & Taylor, S. A. (2023). Hybridization provides climate resilience. *Nature Climate Change*, *13*, 212–213.

Van Rossum, G., & Drake Jr, F. L. (1995). *Python reference manual*. Centrum voor Wiskunde en Informatica Amsterdam.

Vilas, A., Pérez-Figueroa, A., Quesada, H., & Caballero, A. (2015). Allelic diversity for neutral markers retains a higher adaptive potential for quantitative traits than expected heterozygosity. *Molecular Ecology*, *24*(17), 4419–4432.

Wade, A. A., Hand, B. K., Kovach, R. P., Luikart, G., Whited, D. C., & Muhlfeld, C. C. (2017). Accounting for adaptive capacity and uncertainty in assessments of species' climate-change vulnerability. *Conservation Biology*, *31*(1), 136–149.

Wang, I. J., & Bradburd, G. S. (2014). Isolation by environment. *Molecular Ecology*, *23*(23), 5649–5662.

Weiss-Lehman, C., & Shaw, A. K. (2020). Spatial population structure determines extinction risk in climate-induced range shifts. *The American Naturalist*, *195*(1), 31–42.

Williams, J. W., & Jackson, S. T. (2007). Novel climates, no-analog communities, and ecological surprises. *Frontiers in Ecology and the Environment*, *5*(9), 475–482.

Williams, J. W., Jackson, S. T., & Kutzbach, J. E. (2007). Projected distributions of novel and disappearing climates by 2100 AD. *Proceedings of the National Academy of Sciences of the United States of America*, *104*(14), 5738–5742.

Wright, S. (1931). Evolution in Mendelian populations. *Genetics*, *16*, 97–159.

Yeaman, S. (2015). Local adaptation by alleles of small effect. *The American Naturalist*, *186*(S1), S74–S89.

Yeaman, S. (2022). Evolution of polygenic traits under global vs local adaptation. *Genetics*, *220*(1), 134.

Yeaman, S., & Whitlock, M. C. (2011). The genetic architecture of adaptation under migration–selection balance. *Evolution*, *65*(7), 1897–1911.

SUPPORTING INFORMATION

Additional supporting information can be found online in the Supporting Information section at the end of this article.

How to cite this article: Terasaki Hart, D. E., & Wang, I. J. (2024). Genomic architecture controls multivariate adaptation to climate change. *Global Change Biology*, *30*, e17179. https://doi.org/10.1111/gcb.17179

Supporting Information for

Genomic architecture controls multivariate adaptation to climate change

Drew E. Terasaki Hart and Ian J. Wang

Corresponding Author name.
E-mail: drew.hart@berkeley.edu

This PDF file includes:

Figs. S1 to S4
Table S1
Code Sample S1

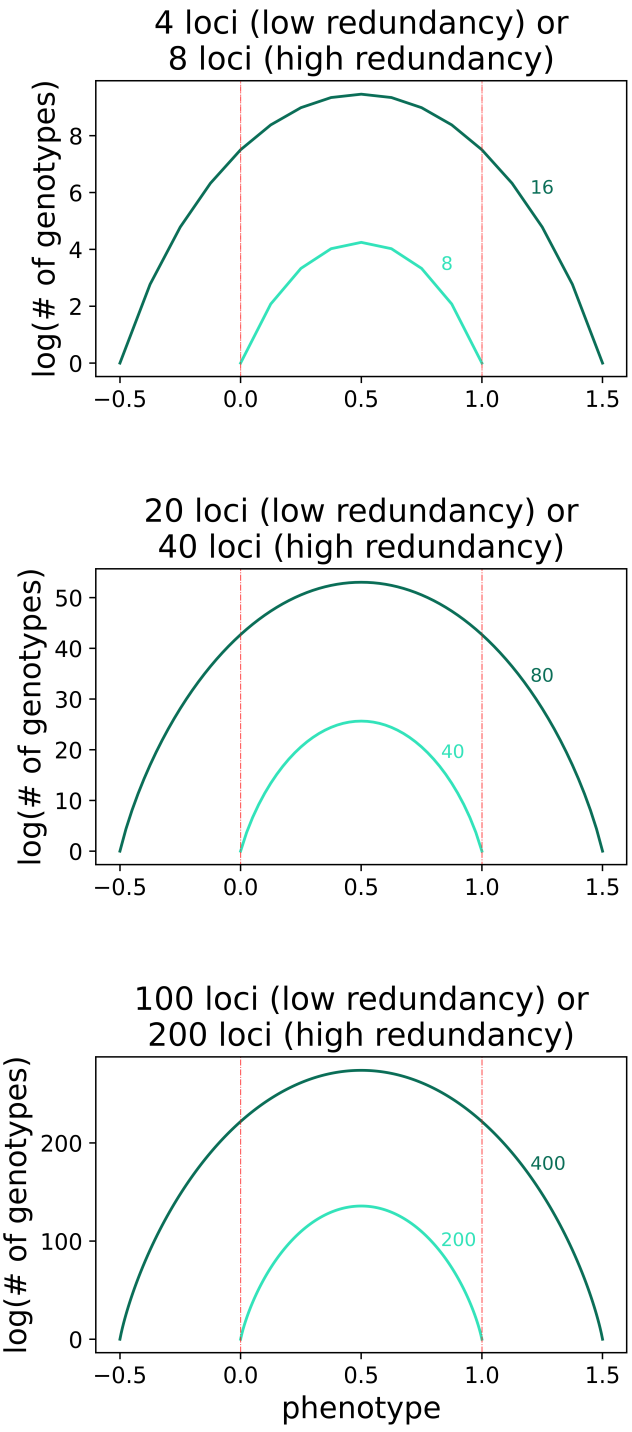

Fig. S1. Plots of the number of genotypes (y-axis) that yield each phenotypic value (x-axis). Polygenicities corresponding to low redundancy scenarios are plotted and labeled in light teal and those corresponding to high redundancy scenarios in dark teal. The minimum and maximum environmental values on the landscape are represented by dashed vertical lines. Plots follow the visualization of genotypic redundancy in Láruson *et al.* 2020 (**?**), Box 1, Figure I.

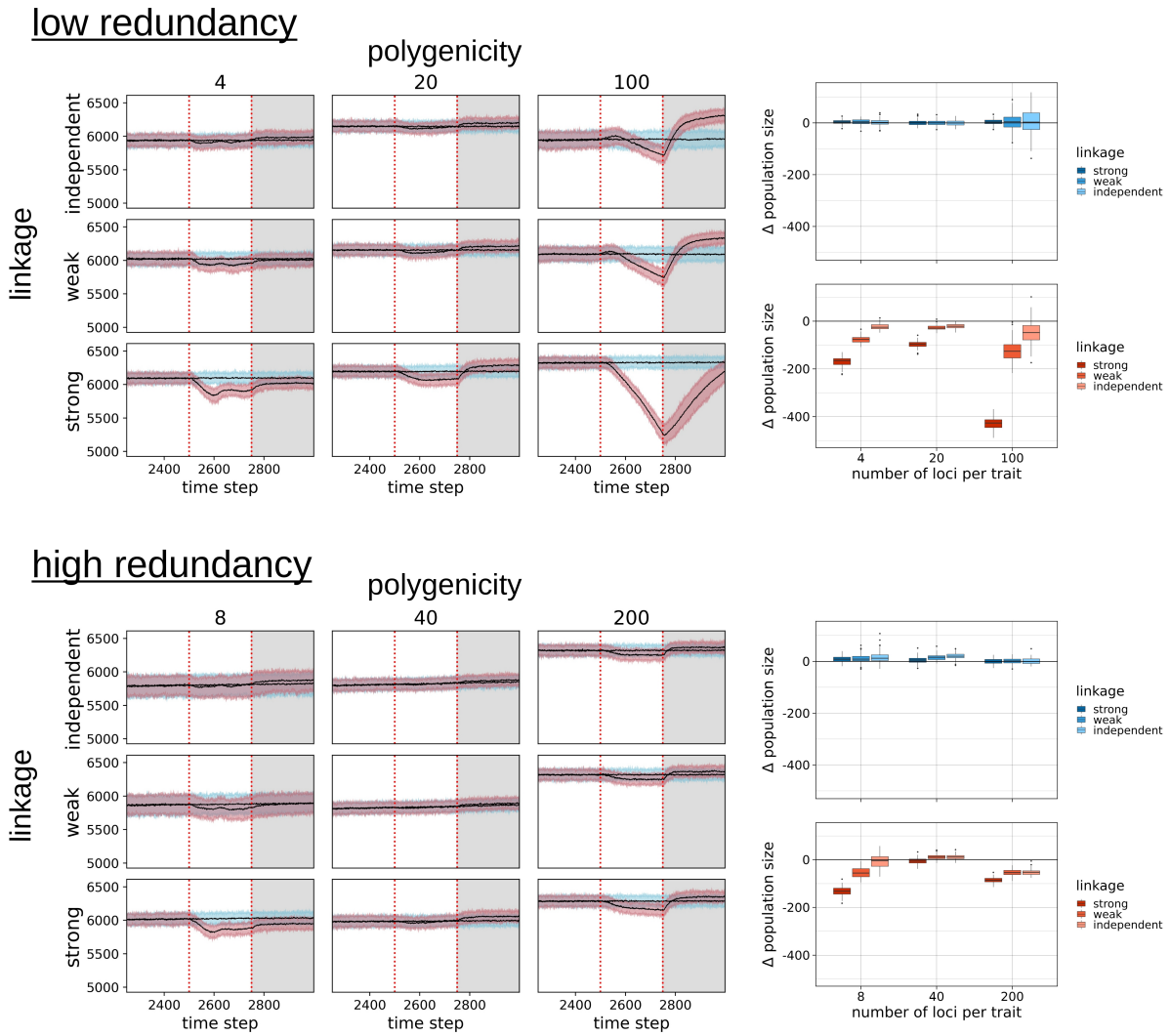

Fig. S2. Left: Population size dynamics for all scenarios during the 250 time steps before, during, and after the climate change period (separated by red, dashed lines). Black lines represent mean values, and the shaded areas represent variability envelopes (5th percentile to 95th percentile) for climate change (red) and null simulations (blue). Right: Boxplots of changes in mean population size during the climate change period for all scenarios. Null scenarios are plotted on the top, in blue, and main scenarios are plotted on the bottom, in red. Within each plot, the scenarios are organized by polygenicity (number of loci per trait) on the x-axis and shaded by the strength of linkage.

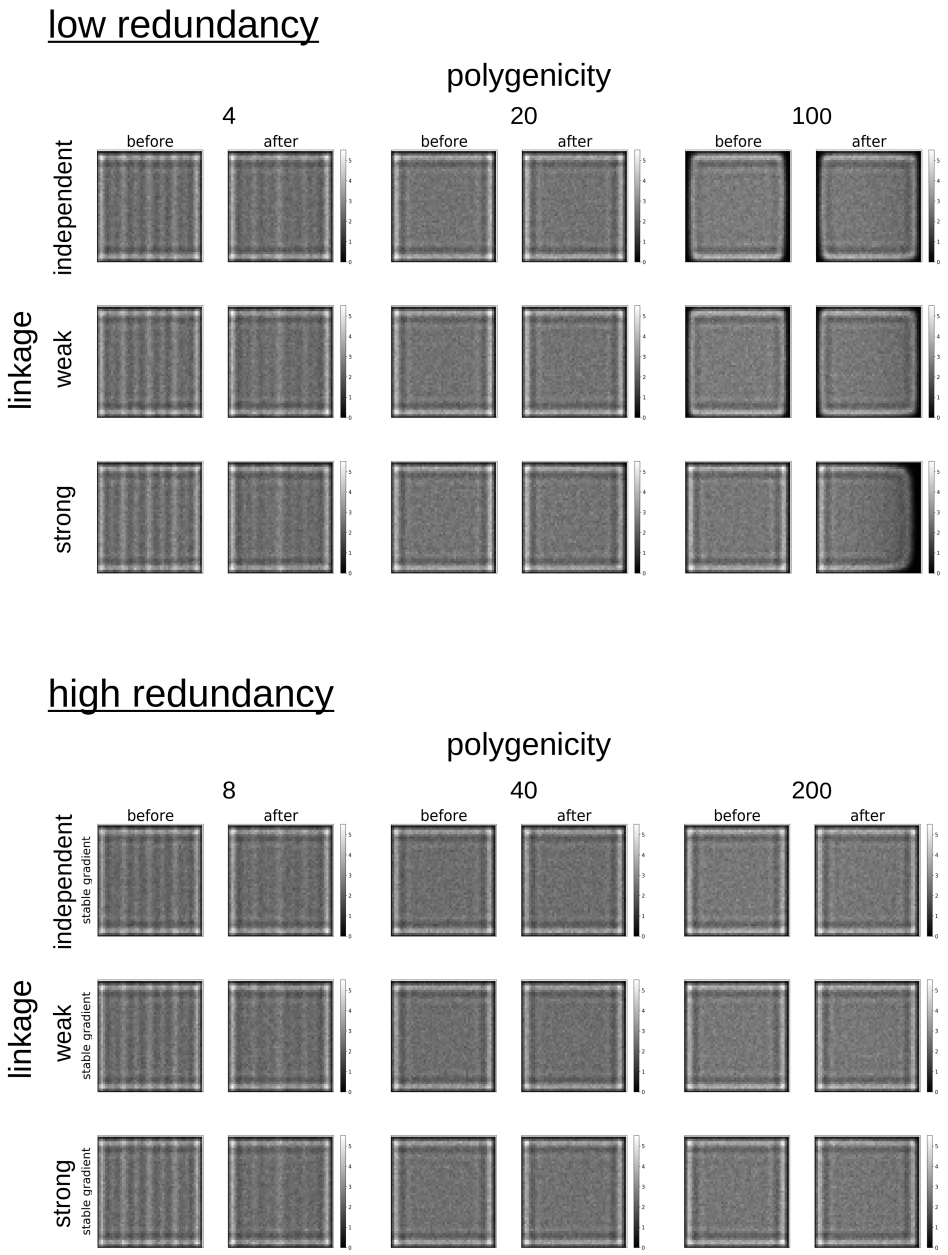

Fig. S3. Maps of population density before and after climate change for all scenarios. In addition to showing local extinction in the low redundancy, high polygenicity, strong linkage scenario (top section, bottom right), these maps also show moderate simulation edge effects and density banding in the low polygenicity scenarios because of the mismatch between environmental and phenotypic resolutions.

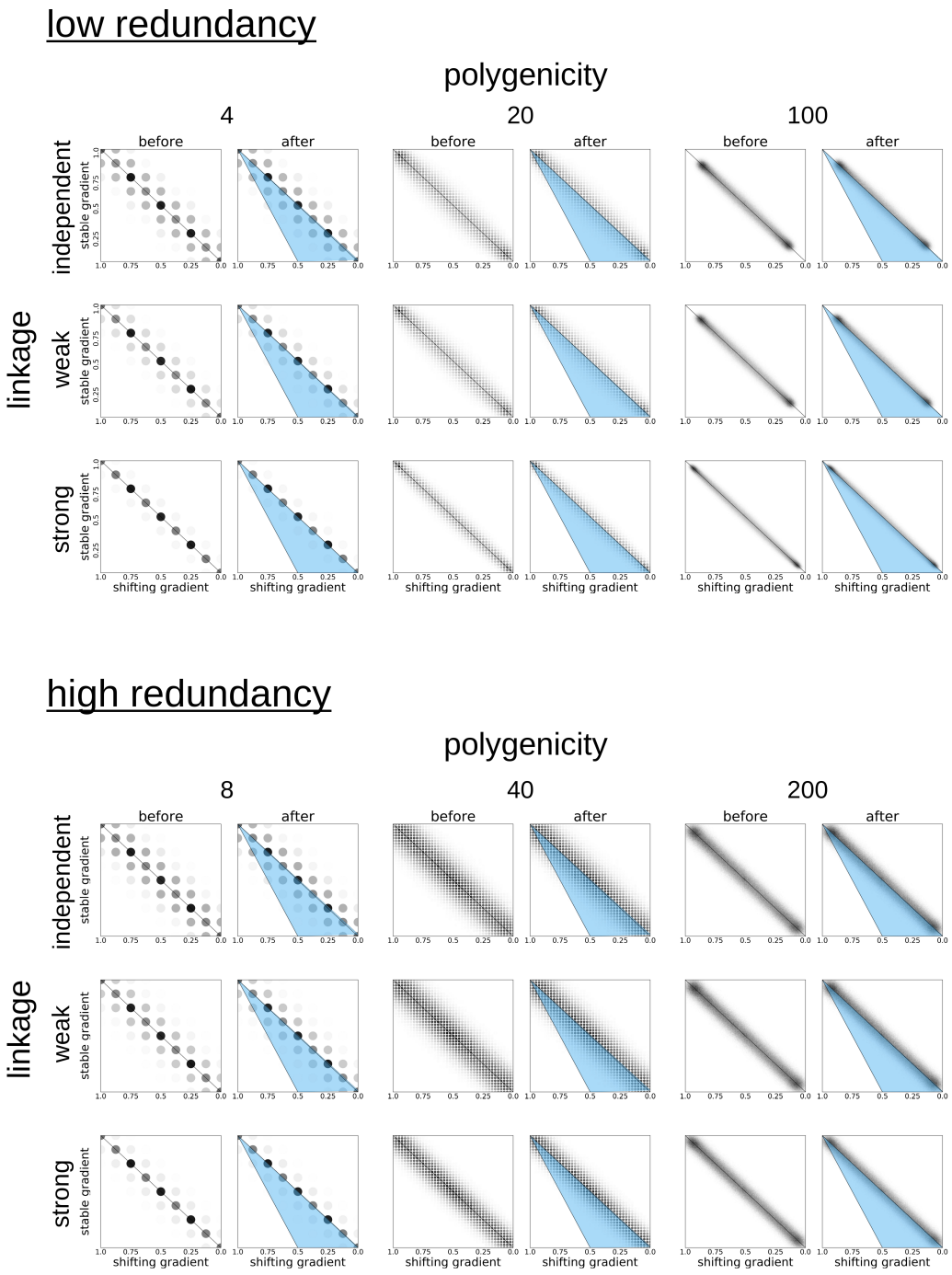

Fig. S4. Scatterplots of the observed versus expected phenotypic shift during the climate change period for all 18 of our simulated scenarios. For each scenario, the left ('before') scatterplot shows the distribution of phenotypes before climate change begins, and the right ('after') scatterplot shows how the distribution has shifted by the end of the climate change period. The trait adapted to the shifting environmental gradient is distributed along the x-axis, with the trait adapted to the stable gradient on the y-axis. The size and opacity of each point represents the number of individuals exhibiting that two-dimensional phenotype. The gridded arrangement of the points in each scatterplot is a function of the number of loci per trait, which determines the set of possible phenotypes. Solid black lines delineate the shifts in the phenotypic distributions' central tendencies that are expected to take place during the climate change period, dotted black lines depict the observed distributions' central tendencies, and blue wedges depict the differences between the expected and observed distributions ('phenotypic shortfall').

Table S1. Predicted main vs. null upslope gene flow (and 95% confidence intervals) for all 18 scenarios.

genicity	linkage	redundancy	predicted gene flow ($\pm$ 95% C.I.)
0	2	1	0.04916 ± 0.00211
1	2	1	0.03496 ± 0.00177
2	2	1	0.02076 ± 0.00211
0	1	1	0.03622 ± 0.00177
1	1	1	0.02202 ± 0.00134
2	1	1	0.00782 ± 0.00177
0	0	1	0.02328 ± 0.00211
1	0	1	0.00908 ± 0.00177
2	0	1	-0.00512 ± 0.00211
0	2	0	0.06470 ± 0.00211
1	2	0	0.05050 ± 0.00177
2	2	0	0.03630 ± 0.00211
0	1	0	0.05176 ± 0.00177
1	1	0	0.03756 ± 0.00134
2	1	0	0.02336 ± 0.00177
0	0	0	0.03883 ± 0.00211
1	0	0	0.02463 ± 0.00177
2	0	0	0.01042 ± 0.00211

Code Sample S1: Template parameters file

```
# template_params.py

import numpy as np
import pandas as pd
import os

# set up the landscape
b4 = np.vstack([np.linspace(1, 0, 50) for _ in range(50)])
af = np.vstack([np.linspace(1, 0.5, 50) for _ in range(50)])
stable = np.vstack([np.linspace(1, 0, 50) for _ in range(50)])
K = np.ones((50,50))

# NOTE: time_steps.CSV USED TO SET CLIMATE CHANGE
#       TO START AT TIME STEP 2500
#       AND FINISH AT TIME STEP 2750
if os.getcwd().split('/')[1] == 'home':
    steps = pd.read_csv(('/home/deth/Desktop/CAL/research/projects/sim/'
                         'ch2/climate_change_adaptation_and_genomic_arch/sim/'
                         'time_steps.CSV'))
else:
    steps = pd.read_csv(('/global/scratch/users/drewhart/'
                         'ch2/climate_change_adaptation_and_genomic_arch/sim/'
                         'time_steps.CSV'))
# set time when environmental change begins
change_T = int(steps[steps['name']=='start']['num'].values[0])
# set time when environmental change ends
T = int(steps[steps['name']=='end']['num'].values[0])

# show the landscape, for debugging, if requested
debug_landscape = False
if debug_landscape:
    import matplotlib.pyplot as plt
    fig = plt.figure()
    ax1 = fig.add_subplot(221)
    im1 = ax1.imshow(b4, cmap='spring', vmin=0, vmax=1)
    plt.colorbar(im1)
    ax3 = fig.add_subplot(223)
    im3 = ax3.imshow(af, cmap='spring', vmin=0, vmax=1)
    plt.colorbar(im3)
    ax2 = fig.add_subplot(222)
    im2 = ax2.imshow(stable, cmap='winter', vmin=0, vmax=1)
    plt.colorbar(im2)
    ax4 = fig.add_subplot(224)
    im4 = ax4.imshow(K, cmap='autumn', vmin=0, vmax=1)
    plt.colorbar(im4)
    plt.show()


# This is a parameters file generated by Geonomics
# (by the gnx.make_parameters_file() function).


                  #   ::::::          :::    :: ::::::::::::#
              #::::::    ::::   :::      ::    :: :: :::::::::: ::#
           #::::::::::     ::            ::   :::::::::::::::::::::::#
         #::::::::::                       :::::::::: :::::: ::::::::  ::#
       #  : ::::  ::                      ::::  : ::    :::::::: : ::  :    #
     # GGGGG :EEEE: OOOOO   NN   NN   OOOOO   MM   MM IIIIII  CCCCC SSSSS #
    # GG     EE    OO   OO  NNN  NN  OO   OO  MM   MM   II   CC     SS     #
    # GG     EE   OO     OO NN N NN OO     OO MMM MMM   II   CC     SSSSSS #
    # GG GGG EEEE OO     OO NN  NNN OO     OO MM M MM   II   CC         SS #
    # GG   G EE    OO   OO  NN   NN  OO   OO  MM   MM   II   CC        SSS #
     # GGGGG :EEEE: OOOOO   NN   NN   OOOOO   MM   MM IIIIII  CCCCC SSSSS #
       #    : ::::::::               :::::::::: ::              ::  :   : #
         #:    :::::                   :::::: :::             :::::::  #
           #    :::                     :::::  ::              ::::: #
              #  ::                      ::::                    #
                   #                                    #
                      #  :: ::    :::            #


params = {
```

```
################################################################################

###################
#### LANDSCAPE ####
###################
    'landscape': {

    ###############
    #### main ####
    ###############
        'main': {
            #x,y (a.k.a. j,i) dimensions of the Landscape
            'dim':                      (50,50),
            #x,y resolution of the Landscape
            'res':                      (1,1),
            #x,y coords of upper-left corner of the Landscape
            'ulc':                      (0,0),
            #projection of the Landscape
            'prj':                      None,
            }, # <END> 'main'

    #################
    #### layers ####
    #################
        'layers': {

            #layer name (LAYER NAMES MUST BE UNIQUE!)
            'shift': {

        #-------------------------------------#
        #--- layer num. 0: init parameters ---#
        #-------------------------------------#

                #initiating parameters for this layer
                'init': {

                    #parameters for a 'defined'-type Layer
                    'defined': {
                        #raster to use for the Layer
                        'rast':                 b4,
                        #point coordinates
                        'pts':                  None,
                        #point values
                        'vals':                 None,
                        #interpolation method {None, 'linear', 'cubic',
                        #'nearest'}
                        'interp_method':        None,

                        }, # <END> 'defined'

                    }, # <END> 'init'

            #---------------------------------------#
            #--- layer num. 0: change parameters ---#
            #---------------------------------------#

                #landscape-change events for this Layer
                'change': {

                    0: {
                        #array or file for final raster of event, or directory
                        #of files for each stepwise change in event
                        'change_rast':            af,
                        #starting timestep of event
                        'start_t':          change_T,
                        #ending timestep of event
                        'end_t':            T,
                        #number of stepwise changes in event
                        'n_steps':          T-change_T,
                        }, # <END> event 0

                    }, # <END> 'change'

                }, # <END> layer num. 0
```

```
    #layer name (LAYER NAMES MUST BE UNIQUE!)
    'stable': {

#-------------------------------------#
#--- layer num. 1: init parameters ---#
#-------------------------------------#

        #initiating parameters for this layer
        'init': {

            #parameters for a 'defined'-type Layer
            'defined': {
                #raster to use for the Layer
                'rast':                 stable,
                #point coordinates
                'pts':                  None,
                #point values
                'vals':                 None,
                #interpolation method {None, 'linear', 'cubic',
                #'nearest'}
                'interp_method':        None,

                }, # <END> 'defined'

            }, # <END> 'init'

        }, # <END> layer num. 1


    #layer name (LAYER NAMES MUST BE UNIQUE!)
    'K': {

#-------------------------------------#
#--- layer num. 2: init parameters ---#
#-------------------------------------#

        #initiating parameters for this layer
        'init': {

            #parameters for a 'defined'-type Layer
            'defined': {
                #raster to use for the Layer
                'rast':                 K,
                #point coordinates
                'pts':                  None,
                #point values
                'vals':                 None,
                #interpolation method {None, 'linear', 'cubic',
                #'nearest'}
                'interp_method':        None,

                }, # <END> 'defined'

            }, # <END> 'init'

        }, # <END> layer num. 2


#layer name (LAYER NAMES MUST BE UNIQUE!)
'move': {

#-------------------------------------#
#--- layer num. 2: init parameters ---#
#-------------------------------------#

        #initiating parameters for this layer
        'init': {

            #parameters for a 'defined'-type Layer
            'defined': {
                #raster to use for the Layer
                'rast':                 np.ones((50,50)),
```

```
                    #point coordinates
                    'pts':                  None,
                    #point values
                    'vals':                 None,
                    #interpolation method {None, 'linear', 'cubic',
                    #'nearest'}
                    'interp_method':        None,

                    }, # <END> 'defined'

                }, # <END> 'init'

            }


    #### NOTE: Individual Layers' sections can be copy-and-pasted (and
    #### assigned distinct keys and names), to create additional Layers.


        } # <END> 'layers'

    }, # <END> 'landscape'


################################################################################

####################
#### COMMUNITY ####
####################
    'comm': {

        'species': {

            #species name (SPECIES NAMES MUST BE UNIQUE!)
            'spp_0': {

            #-----------------------------------#
            #--- spp num. 0: init parameters ---#
            #-----------------------------------#

                'init': {
                    #starting number of individs
                    'N':                1000,
                    #carrying-capacity Layer name
                    'K_layer':          'K',
                    #multiplicative factor for carrying-capacity layer
                    'K_factor':         2.5,
                    }, # <END> 'init'

            #-----------------------------------#
            #--- spp num. 0: mating parameters ---#
            #-----------------------------------#

                'mating'    : {
                    #age(s) at sexual maturity (if tuple, female first)
                    'repro_age':            0,
                    #whether to assign sexes
                    'sex':                  False,
                    #ratio of males to females
                    'sex_ratio':            1/1,
                    #whether P(birth) should be weighted by parental dist
                    'dist_weighted_birth':   False,
                    #intrinsic growth rate
                    'R':                    0.5,
                    #intrinsic birth rate (MUST BE 0<=b<=1)
                    'b':                    0.5,
                    #expectation of distr of n offspring per mating pair
                    'n_births_distr_lambda':    1,
                    #whether n births should be fixed at n_births_dist_lambda
                    'n_births_fixed':           True,
                    #radius of mate-search area
                    'mating_radius':            5,
                        #whether individs should choose nearest neighs as mates
                    'choose_nearest_mate':      False,
```

```
            #whether mate-choice should be inverse distance-weighted
        'inverse_dist_mating':      False,
        }, # <END> 'mating'

#---------------------------------------#
#--- spp num. 0: mortality parameters ---#
#---------------------------------------#

    'mortality'     : {
        #maximum age
        'max_age':                      None,
        #min P(death) (MUST BE 0<=d_min<=1)
        'd_min':                        0,
        #max P(death) (MUST BE 0<=d_max<=1)
        'd_max':                        1,
        #width of window used to estimate local pop density
        'density_grid_window_width':    None,
        }, # <END> 'mortality'

#---------------------------------------#
#--- spp num. 0: movement parameters ---#
#---------------------------------------#

    'movement': {
        #whether or not the species is mobile
        'move':                     True,
        #mode of distr of movement direction
        'direction_distr_mu':       0,
        #concentration of distr of movement direction
        'direction_distr_kappa':    0,
        #mean of distr of movement distance
        'movement_distance_distr_param1':        0.25,
        #variance of distr of movement distance
        'movement_distance_distr_param2':     0.5,
            #movement distance distr to use ('lognormal','levy','wald')
        'movement_distance_distr':             'wald',
        #mean of distr of dispersal distance
        'dispersal_distance_distr_param1':       0.5,
        #variance of distr of dispersal distance
        'dispersal_distance_distr_param2':    0.5,
            #dispersal distance distr to use ('lognormal','levy','wald')
        'dispersal_distance_distr':             'wald',
        },    # <END> 'movement'


#---------------------------------------------------#
#--- spp num. 0: genomic architecture parameters ---#
#---------------------------------------------------#

    'gen_arch': {
        #file defining custom genomic arch
        'gen_arch_file':            None,
        #num of loci
        'L':                        1000,
        #value to use for fixed starting allele freqs (None to draw)
        'start_p_fixed':            0.5,
        #whether to start neutral locus freqs at 0
        'start_neut_zero':          True,
        #genome-wide per-base neutral mut rate (0 to disable)
        'mu_neut':                  0,
        #genome-wide per-base deleterious mut rate (0 to disable)
        'mu_delet':                 0,
        #shape of distr of deleterious effect sizes
        'delet_alpha_distr_shape':  0.2,
        #scale of distr of deleterious effect sizes
        'delet_alpha_distr_scale':  0.2,
        #NOTE: MAIN SCRIPT OVERRIDES THE FOLLOWING TWO PARAMS
        #TO SET RECOMBINATION RATES TO A FIXED VALUE OF
        #0.5, 0.05, OR 0.005 FOR INDEPENDENT,
        #WEAK, OR STRONG LINKAGE VALUES
        #alpha of distr of recomb rates
        'r_distr_alpha':            1000,
        #beta of distr of recomb rates
        'r_distr_beta':             1e3,
```

```
#whether loci should be dominant (for allele '1')
'dom':                      False,
#whether to allow pleiotropy
'pleiotropy':               False,
#custom fn for drawing recomb rates
'recomb_rate_custom_fn':    None,
#number of recomb paths to hold in memory
'n_recomb_paths_mem':       int(1e4),
#total number of recomb paths to simulate
'n_recomb_paths_tot':       int(1e5),
    #num of crossing-over events (i.e. recombs) to simulate
'n_recomb_sims':            100_000,
#whether to generate recombination paths at each timestep
'allow_ad_hoc_recomb':       False,
#whether to save mutation logs
'mut_log':                  False,
    #whether to jitter recomb bps, to correctly track num_trees
'jitter_breakpoints': False,
   #whether to use tskit (to record full spatial pedigree)
'use_tskit': True,
     #time step interval for simplication of tskit tables
'tskit_simp_interval': 100,

'traits': {

    #-------------------------#
    #---trait 0 parameters ---#
    #-------------------------#
    #trait name (TRAIT NAMES MUST BE UNIQUE!)
    'trait_0': {
        #trait-selection Layer name
        'layer':                'shift',
        #polygenic selection coefficient
        'phi':                  1,
        #NOTE: MAIN SCRIPT CHANGES NEXT PARAM TO 4, 20, OR 100
        #FOR LOW-REDUNDANCY SCENARIOS OF DIFF. POLYGENICITY,
        #OR 8, 40, OR 200 FOR HIGH-REDUNDANCY SCENARIOS
        #number of loci underlying trait
        'n_loci':               50,
        #mutation rate at loci underlying trait
        'mu':                   0,
        #mean of distr of effect sizes
        'alpha_distr_mu' :      0,
        #variance of distr of effect size
        'alpha_distr_sigma':    0,
        #max allowed magnitude for an alpha value
        'max_alpha_mag':        None,
        #curvature of fitness function
        'gamma':                1,
        #whether the trait is universally advantageous
        'univ_adv':             False
        }, # <END> trait 0

    #-------------------------#
    #---trait 1 parameters ---#
    #-------------------------#
    #trait name (TRAIT NAMES MUST BE UNIQUE!)
    'trait_1': {
        #trait-selection Layer name
        'layer':                'stable',
        #polygenic selection coefficient
        'phi':                  1,
        #NOTE: MAIN SCRIPT CHANGES NEXT PARAM TO 4, 20, OR 100
        #FOR LOW-REDUNDANCY SCENARIOS OF DIFF. POLYGENICITY,
        #OR 8, 40, OR 200 FOR HIGH-REDUNDANCY SCENARIOS
        #number of loci underlying trait
        'n_loci':               50,
        #mutation rate at loci underlying trait
        'mu':                   0,
        #mean of distr of effect sizes
        'alpha_distr_mu' :      0,
        #variance of distr of effect size
        'alpha_distr_sigma':    0,
        #max allowed magnitude for an alpha value
```

```
                            'max_alpha_mag':        None,
                            #curvature of fitness function
                            'gamma':                1,
                            #whether the trait is universally advantageous
                            'univ_adv':             False
                            }, # <END> trait 1


    #### NOTE: Individual Traits' sections can be copy-and-pasted (and
    #### assigned distinct keys and names), to create additional Traits.


                        }, # <END> 'traits'

                    }, # <END> 'gen_arch'


                }, # <END> spp num. 0



    #### NOTE: individual Species' sections can be copy-and-pasted (and
    #### assigned distinct keys and names), to create additional Species.


            }, # <END> 'species'

        }, # <END> 'comm'


################################################################################

###############
#### MODEL ####
###############
    'model': {
        # NOTE: NEXT PARAM OVERRIDDEN BY MAIN SCRIPT
        #total Model runtime (in timesteps)
        'T':            100000,
        #min burn-in runtime (in timesteps)
        'burn_T':       30,
        #seed number
        'num':          None,

        ################################
        #### iterations parameters ####
        ################################
        'its': {
            #num iterations
            'n_its':            1,
            #whether to randomize Landscape each iteration
            'rand_landscape':   False,
            #whether to randomize Community each iteration
            'rand_comm':        False,
              #whether to randomize GenomicArchitectures each iteration
            'rand_genarch':     True,
            #whether to burn in each iteration
            'repeat_burn':      False,
            }, # <END> 'iterations'


        ####################################
        #### data-collection parameters ####
        ####################################
        'data': {
            'sampling': {
                #sampling scheme {'all', 'random', 'point', 'transect'}
                'scheme':               'all',
                #sample size at each point, for point & transect sampling
                'n':                    1000,
                #coords of collection points, for point sampling
                'points':               None,
                #coords of transect endpoints, for transect sampling
                'transect_endpoints':   None,
```

```
            #num points along transect, for transect sampling
            'n_transect_points':    None,
            #collection radius around points, for point & transect sampling
            'radius':               None,
            #when to collect data
            'when':                [change_T-1,
                                    int((change_T-1+T-1)/2),
                                    T-1],
            #whether to save current Layers when data is collected
            'include_landscape':    False,
            #whether to include fixed loci in VCF files
            'include_fixed_sites':  True,
            },
        'format': {
            #format for genetic data {'vcf', 'fasta'}
            'gen_format':           ['vcf'],
            #format for vector geodata {'csv', 'shapefile', 'geojson'}
            'geo_vect_format':      'csv',
            #format for raster geodata {'geotiff', 'txt'}
            'geo_rast_format':      'geotiff',
               #format for files containing non-neutral loci
            'nonneut_loc_format':      'csv',
            },
        }, #<END> 'data'

    } # <END> 'model'

} # <END> params
```